

**NUMERICAL SIMULATION OF DEFORMATION
BANDS IN POROUS SANDSTONE: A CASE STUDY OF
DHOK PATHAN FORMATION (PAKISTAN)**



BY

ILTAF AHMAD

**NATIONAL CENTRE OF EXCELLENCE IN GEOLOGY
UNIVERSITY OF PESHAWAR**

2012

بِسْمِ اللَّهِ الرَّحْمَنِ الرَّحِيمِ

**In the name of
ALLAH
the most Beneficent, the most Merciful**

**NUMERICAL SIMULATION OF DEFORMATION
BANDS IN POROUS SANDSTONE: A CASE STUDY OF
DHOK PATHAN FORMATION (PAKISTAN)**



BY

ILTAF AHMAD

*Thesis submitted to the National Center of Excellence in Geology,
University of Peshawar in partial fulfillment of the requirements for the
degree of Master of Philosophy in Geology*

**NATIONAL CENTRE OF EXCELLENCE IN GEOLOGY
UNIVERSITY OF PESHAWAR**

2012

APPROVED BY



(Examiner)

Dr. Ishtiaq Jadoon

Professor & Chairman

Department of Environmental Sciences CITT

COMSATS Institute of Information Technology

University Road, Toba Camp

Abottabad.



(Supervisor)

Dr. Muhammad Sayab

National Centre of Excellence in Geology

University of Peshawar

Peshawar



(Co-Supervisor)

Dr. Iqbal Qaiser

Assistant Professor

Deptt. of Civil Engineering

University of Engineering & Technology

Peshawar.



(Director)

Prof. Dr. M. Asif Khan (T.I)

National Centre of Excellence in Geology

University of Peshawar

Peshawar

ABSTRACT

Deformation bands are low-displacement deformed zones in a ‘conjugate’ or ‘Riedel’ pattern that increase cohesion and reduce porosity and permeability. Intersecting shear fractures that have opposite senses of slip and have an acute angle ($\sim 60^\circ$) that is bisected by the maximum compressive stress (σ_1) at the time of fracturing are called ‘conjugate’ fractures. The term ‘Riedel’ refers to a set of en-echelon fracture segments of synthetic R and antithetic R' shears oriented at low- and high- angles to the main strike-slip fault zone, respectively. Both ‘conjugate’ and ‘Riedel’ patterns in sandstone have been documented in many studies and considerable amount of theoretical work in terms of their formation mechanism has been carried out. In this study, numerical modeling is performed to analyze the nucleation and sequential growth of deformation bands in a sandstone sample collected from the Dhok Pathan Formation, Surghar-Shinghar Range. These rocks preserve excellent exposure of ‘conjugate’ and ‘Riedel’ deformation band geometries. The advantage of numerical over other modeling techniques is that it allows user to model any particular physical/geological phenomenon and associated problem in various steps that follow sets of executable commands based on pre-defined mathematical equations. The executable commands are written in a meaningful semantics that lead to answerable simulation. The results can be directly comparable to given physical process/problem at any stage with an advantage of quantitative outputs. Finite Difference Code (FDC) of Itasca Inc., is used to simulate the structural evolution of deformation bands in the Dhok Pathan sandstone. To generate model steps, FDC requires mechanical properties of sandstone that is an essential ingredient of the data file for execution. In this regard, the mechanical properties of

porous sandstone are very carefully taken from the literature and used for modeling purposes. In order to simulate deformation bands Mohr-Coulomb constitutive model was adopted. As assumed in theoretical models, lateral shear (strike-slip) was applied to the pre-defined mesh. However, no 'Riedel' geometries were formed at any stage during the given number of steps. After closely analyzing the analogue models, force/load (σ_1) was applied on top of the mesh and observed the nucleation of 'conjugate' pattern. The developed pattern consists of two cross-cutting sets oriented at an acute angle ($\sim 70^\circ$) to σ_1 and each individual set produced considerable thickness (12 m). In addition, each set vaguely exhibits a zone with antithetic pattern oriented at $\sim 70^\circ$. We propose that this pattern may be the manifestation of R' shear. The conjugate set form in response to 200×10^9 Pa stresses (σ_1) in sandstone. The results of this study are novel to understand 'step-by-step' tectonic evolution of deformation bands using numerical approach.

Dedication

This research work is lovingly dedicated to my parents who have been a constant source of inspiration for me. They have given me the drive and discipline to tackle any task with enthusiasm and determination. Without their love and support this project would not have been made possible.

Iltaf Ahmad

ACKNOWLEDGEMENTS

All praise to almighty ALLAH, the source of all knowledge, wisdom within and beyond our comprehension. Great thanks to ALLAH, who gave me the strength and enabled me to overcome the difficulties that I faced during the completion of this work.

First and foremost I offer my sincerest gratitude to my supervisor, Dr. Muhammad Sayab, who has supported me throughout my thesis with his patience and knowledge whilst allowing me the room to work in my own way. I attribute the level of my M.Phil degree to his encouragement and effort without which this thesis would not have been completed.

I extend my heartily thanks to my co-supervisor, Dr. Qaiser Iqbal, whose encouragement, guidance and support from the initial to the final level enabled me to develop better understanding of the subject. His caring attitude and fruitful guidance will always be appreciated.

Words can hardly suffice to express depth of gratitude I owe for Prof. Dr. M. Tahir Shah, Graduate student advisor, NCEG, university of Peshawar, who has always been kind and supportive. I would like to thank Mr. Muhammad Waseem (Research Associate) for his assistance and useful discussion. I would especially like to thank Mr. Muhammad Riaz (Assistant Professor NCEG) who was always helpful when, in several crucial moments in my study, I was beset with project-related problems and for sharing his knowledge and experience. I am extremely thankful to Mr. Shahid Waheed (Network administrator) for solving the software related problems.

It will be injustice if I do not mention here the names of my friends especially Mr. Qazi Yasar Hamid (Assistant Director GSP), Dr. Syed Zahid Shah (Senior

Scientist PAEC), Islam Uddin, Miss Nida Gul, Asim Israr, Syed Ali Turab, Waheedullah, Khalid Latif and Said Muhammad for their assistance throughout this work. I am grateful to all my friends and colleagues.

Finally, this work is highly acknowledged to all my family members specially Khan Baba (Abba G) and Ammi G. They deserve regards and special thanks for their love, moral and financial support throughout my studies, without whom help I may not have been able to achieve my goals. May God bless them and may God give me a chance to serve them better (Aamin).

Iltaf Ahmad

March 10, 2012

LIST OF CONTENTS

CONTENTS	PAGE NO.
ABSTRACT	iii
ACKNOWLEDGEMENTS	vi
LIST OF CONTENTS	viii
LIST OF ILLUSTRATIONS	xii
LIST OF TABLES	xvii
1. CHAPTER#1 INTRODUCTION	1
1.1. General description	1
1.1.1. Types of deformation bands	1
1.1.2. Characteristics of deformation bands	3
1.1.3. Comparison with ordinary faults	4
1.2. Purpose of investigation	5
1.3. Numerical modeling	7
1.4. Geological setting of the area	8
1.5. Stratigraphy of the Surghar-Shinghar Range	9
1.5.1. Dhok Pathan Formation	10
1.6. Aims and objectives	12
1.7. Methodology	12
1.7.1. Mechanical properties of material	14
1.7.2. FLAC-2D: data file and execution	15
1.8. Significance	16

2. CHAPTER#2	'CONJUGATE' AND 'RIEDEL' DEFORMATION BAND PATTERNS	17
2.1.	Introduction	17
2.2.	Mechanism of the formation of deformation bands	19
2.2.1.	Controlling factors of the deformation bands	21
2.3.	Previous work	21
3. CHAPTER#3	NUMERICAL SIMULATION OF DEFORMATION BANDS	23
3.1.	Introduction	23
3.2.	FLAC-2D	23
3.2.1.	Introduction	23
3.2.2.	Material models	24
3.2.3.	FLAC-2D operation	25
3.2.4.	FLAC applications	26
3.3.	Numerical modeling of the 'Conjugate' and 'Riedel' deformation bands	26
3.4.	Experiment 1	27
3.4.1.	Mesh size and boundary conditions	27
3.4.2.	Material properties	27
3.4.3.	Model run	28
3.4.4.	Resultant geometry	28
3.5.	Experiment 2	29
3.5.1.	Mesh size and boundary conditions	29
3.5.2.	Model run	30
3.5.3.	Resultant geometry	30

3.6.	Experiment 3	30
3.6.1.	Mesh size and boundary conditions	30
3.6.2.	Model run	31
3.6.3.	Resultant geometry	31
3.7.	Experiment 4	31
3.7.1.	Mesh size and boundary conditions	31
3.7.2.	Material properties	32
3.7.3.	Model run	32
3.7.4.	Resultant geometry	32
3.8.	Experiment 5	34
3.8.1.	Mesh size and boundary conditions	34
3.8.2.	Material properties	34
3.8.3.	Model run	35
3.8.4.	Resultant geometry	35
3.9.	Experiment 6	36
3.9.1.	Mesh size and boundary conditions	37
3.9.2.	Model run	37
3.9.3.	Resultant geometry	37
3.10.	Experiment 7	38
3.10.1.	Mesh size and boundary conditions	38
3.10.2.	Model run	39
3.10.3.	Resultant geometry	39
3.11.	Experiment 8	40
3.11.1.	Model run	40
3.11.2.	Resultant geometry	40

3.12. Experiment 9	46
3.12.1. Mesh size and boundary conditions	46
3.12.2. Material properties	46
3.12.3. Model run	46
3.12.4. Resultant geometry	47
3.13. Experiment 10	48
3.13.1. Mesh size and boundary conditions	48
3.13.2. Model run and results	48
3.14. Tabular comparison of experiments	50
4. CHAPTER#4 RESULTS AND COMPARISONS	53
4.1. Comparison with other models	59
4.1.1. Comparison with the field models	59
4.1.2. Comparison with the numerical model of Hobbs & Ord (1989)	60
5. CHAPTER#5 DISCUSSION AND CONCLUSIONS	62
6. REFERENCES	64- 70

LIST OF ILLUSTRATIONS

Fig. No	Description	Page No.
Fig. 1.1	Kinematic classification of deformation bands.	2
Fig. 1.2	(a) Discontinuous fault surface with distinct slip, and (b) continuous displacement characterizing deformation band.	4
Fig. 1.3	(a) Sketch showing a single deformation band, and (b, c) a zone of deformation bands with slip surfaces.	4
Fig. 1.4	Location map of the Himalaya of the north Pakistan and northwestern India showing the major faults and mountain ranges.	6
Fig. 1.5	Photograph showing the coarse grained, moderately sorted, comparatively less compacted sandstone of the Dhok Pathan Formation.	11
Fig. 1.6	Photograph showing hard sandstone bands in the light grey, highly compacted, well-sorted and massive sandstone of the Dhok Pathan Formation.	11
Fig. 1.7	Deformation bands in a porous sandstone sample from the Dhok Pathan Formation, Surghar-Shinghar Range.	13
Fig. 1.8	Triaxial compression results of sandstone.	13
Fig. 2.1	(a) Block diagram showing the fundamental geometric relations of the 'conjugate' deformation bands and 'Riedel' systems, and (b) map view of the 'Riedel' shear zone formed in a clay cake model.	18
Fig. 2.2	Schematic sketch showing a 'Riedel' shear zone composed of R and R' shears linked by transfer zone.	18

Fig. 2.3	Drawing of the common elements within an ideal ‘Riedel’ shear system.	19
Fig. 2.4	Idealized sequential development of deformation band zone in porous sandstone.	20
Fig. 2.5	Photograph showing NW-SE trending shear zone and associated ‘Riedel’ deformation bands from the Dhok Pathan Formation of the Surghar-Shinghar Range (Photo after Kamran, Ahmad and Islam., 2006).	22
Fig. 3.1	(a) Mesh before applying the boundary conditions, and (b) geometry of the mesh after applying the boundary conditions.	29
Fig. 3.2	Mesh before applying the boundary conditions.	30
Fig. 3.3	Geometry of the mesh after applying the boundary conditions.	30
Fig. 3.4	(a) Mesh before applying the boundary conditions, (b) mesh remains undeformed after applying the boundary conditions and execution.	31
Fig. 3.5	Behaviour of the mesh remains unchanged before and after applying the boundary conditions.	33
Fig. 3.6	Displacement vectors plot showing the slippage of velocity at the top and bottom surfaces without shearing the internal geometry of the model.	33
Fig. 3.7	Velocity vectors plot showing little variation of velocity.	34
Fig. 3.8	Mesh remains undisturbed though the variation command (VAR) was applied for velocity variations.	36
Fig. 3.9	Maximum shear strain increment plot showing the incremental distribution of strain but not enough to deform the mesh.	36

Fig. 3.10	Homogeneous mesh before applying the boundary conditions.	37
Fig. 3.11	Initial stage of ‘conjugate’ pattern developed in the homogeneous mesh after applying the boundary conditions and deformation in experiment No. 6.	38
Fig. 3.12	Deformed grid showing the initial stage of the development of cross-cutting sets. Deformation occurs in the mesh by varying load from 200×10^3 Pa to 200×10^8 Pa.	39
Fig. 3.13	Development of ‘conjugate’ pattern with variable load from 200×10^2 Pa to 200×10^9 Pa. Note that the deformation bands are not discrete slip surfaces, rather they form zone with ‘continuous’ deformation as proposed in the theoretical models.	40
Fig. 3.14	Deformed grid after applying the load and execution. ‘Conjugate’ pattern developed at $\sim 70^\circ$.	42
Fig. 3.15	(a) Displacement vectors plot showing the ‘conjugate’ pattern. This plot is significant in terms of determining sense of displacement and is consistent with the ‘conjugate’ shear movement. (b) Velocity vectors plot showing the conjugate pattern and distribution of the velocity vectors inside the mesh.	42
Fig. 3.16	(a) Distribution of principal stresses in the mesh, and (b) shear strain increment plot showing the strain localization.	43
Fig. 3.17	(a) Y-displacement contour plot contour interval is 5.00×10^{-01} , (b) X-displacement contour plot contour interval is 5.00×10^{-01} . Both these plots depict the formation of ‘conjugate’ pattern.	44

Fig. 3.18	(a) Boundary plot of x-component of velocity, (b) boundary plot of Y-component of velocity. Both these plots depict the formation of ‘conjugate’ pattern.	45
Fig. 3.19	Shear strain increment plot showing the well-developed ‘conjugate’ geometries. Here ‘Riedel’ shears are not visible due to their millimeter scale size.	47
Fig. 3.20	Maximum shear strain increment plot showing the strain distribution in mesh.	49
Fig. 4.1	Graph showing the geometry of the mesh before applying the boundary conditions and execution.	54
Fig. 4.2	Geometry of mesh after applying the boundary conditions and execution. Internal geometry of the mesh remains undisturbed.	54
Fig. 4.3	Experimental results on cylindrical marble at room temperature. A. longitudinal fracturing at confining pressure $P=0.1$ MPa, B. single shear fracture at $P=3.5$ MPa, C. conjugate sets at $P=35$ MPa, D. ductile flow at $P=100$ MPa (From Patterson 1978).	55
Fig. 4.4	Graph showing the geometry of 100x100 m mesh before applying the boundary conditions and execution.	57
Fig. 4.5	Deformed grid after applying the load and execution. Applied load varies from 200×10^2 Pa to 200×10^9 Pa at the top and bottom surfaces. ‘Conjugate’ pattern developed at $\sim 70^\circ$. Thickness of individual deformation band set is almost 12 m.	57
Fig. 4.6	‘Riedel’ fracture pattern in deformation band shear zones, Qabul khel area (sayab et al. 1999).	58

Fig. 4.7 Comparison between the model proposed by Davis et al. (1999) based on field measurements and numerically-generated 'conjugate' pattern. 60

Fig. 4.8 Comparison between the numerical model generated by Hobbs and Ord (1989) using constant velocity to shorten the mesh and our model of deformation bands in which variable load (200×10^2 Pa to 200×10^9 Pa) was applied to deform mesh. 61

LIST OF TABLES

Table No.	Description	Page No.
Table 1.1	Table showing the stratigraphy of the Surghar-Shinghar Range.	9
Table 3.1.	Table showing the material properties used for experiment 1.	28
Table 3.2.	Table showing the material properties used for experiment 4.	32
Table 3.3.	Table showing the material properties used in experiment 5.	35
Table 3.4	Table showing the variation in mechanical properties.	51
Table 3.5	Table showing the comparison between the mesh size, material model, strain mode and the number of steps for which solution was attained.	52

CHAPTER - 1

INTRODUCTION

CHAPTER 1

INTRODUCTION

1.1. General description

Deformation in the upper crust is characterized by brittle faulting and associated folding. Depending on the intensity of deformation and rheological properties, several mechanisms are associated with faulting, e.g. fault breccias with angular clasts are the products of low intensity brittle failure, whereas gouge zones indicate high intensity brittle failure (Billi et al., 2003). Similarly, ‘Riedel’ and ‘conjugate’ fracture pattern is indicative of the beginning of incipient shear zone (Ahlgren, 2001).

Deformation bands are one kind of frictional deformation structures in the uppermost Earth’s crust and are precursors to frictional slip (i.e. faulting) in porous granular rocks (Aydin, 1978; Antonellini et al., 1994). Deformation bands first described by Aydin (1978) may be defined as “low-displacement deformed zones in porous rocks that increase cohesion and reduce porosity and permeability as compared to other shear fractures” (Antonellini and Aydin, 1994). These are tabular structures of finite width resulting from strain localization commonly found in compact sand and porous sandstone. Deformation bands exist as a single plane to extensive shear zones with a width of few mm to many meters (Antonellini et al., 1994; Davis et al., 1999).

1.1.1. Types of deformation bands

Kinematically, deformation bands can be classified into three classes:

- (1) Simple shear bands/Deformation band faults (deformation bands with clear shear offset). According to the degree of grain fragmentation and clay content, deformation band faults are further subdivided into three groups (Antonellini et al., 1994):
- a) Deformation band faults with little or no cataclasis,
 - b) Deformation band faults with cataclasis, and
 - c) Deformation band faults with clay smearing.
- (2) Compaction bands (bands of localized porosity reduction and lack shear offset).
- (3) Dilation bands (bands of localized increase in porosity and lack shear offset)
- (Fig. 1.1).

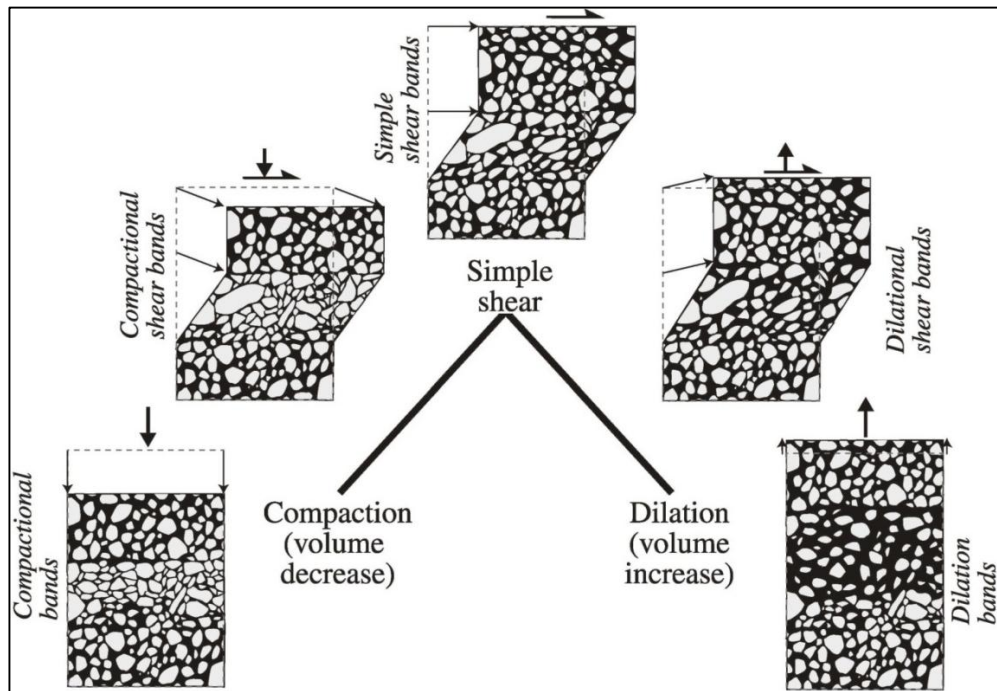


Fig. 1.1. Kinematic classification of deformation bands (Aydin et al., 2006).

Deformation band faults are typically about 1 mm wide and mm to many cm scale long, roughly planar deformation structures that show shear deformation. The slip-to fault-length ratios are low as compared to ordinary faults with slip surfaces in dense lithologies (Fossen and Hesthammer, 1997).

1.1.2. Characteristics of deformation bands

According to Fossen et al. (2007), the important characteristics of the deformation bands in porous rocks are as follows:

- a. Deformation bands are restricted to porous sandstones. The formation and evolution of a deformation band involves a significant amount of grain rotation and translation and this process requires a certain amount of inherited porosity, which is common in sandstones.
- b. A deformation band very rarely represents a discrete slip surface (Fig. 1.2a). Slip surface commonly form at the edge of zones of deformation bands and represents a more mature stage in the development of deformation band faults (Fig. 1.2b).
- c. Deformation bands occur hierarchically as individual bands or as zones of bands associated with slip surfaces (also known as faulted deformation bands, Fig. 1.3).
- d. Individual deformation bands rarely host offsets greater than a few centimeters even when the bands themselves are 100 meter long.
- e. Deformation bands are mainly found at upper-crustal levels.

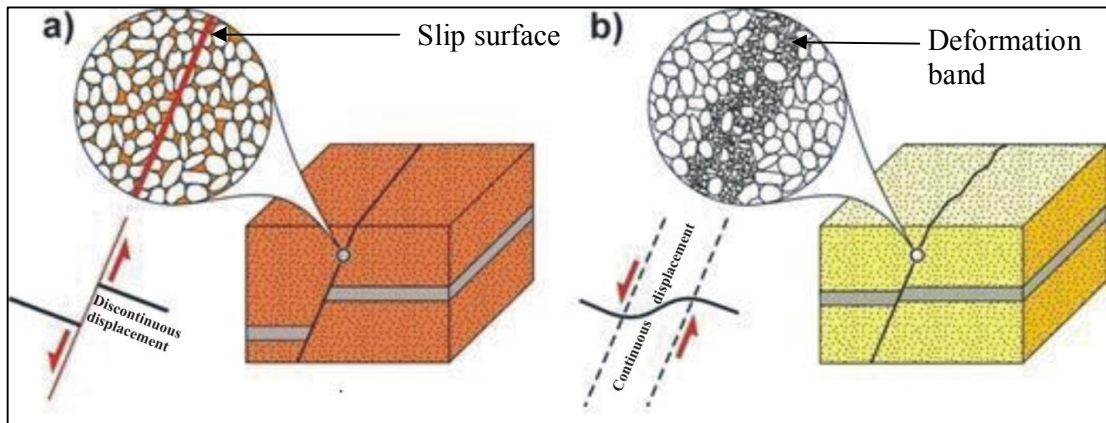


Fig. 1.2. (a) Discontinuous fault surface with distinct slip, and (b) continuous displacement characterizing deformation band.
<http://www.ig.tuwien.ac.at/forschung/schwerpunkte/deformation-mechanism-in-porous-sediments.html>.

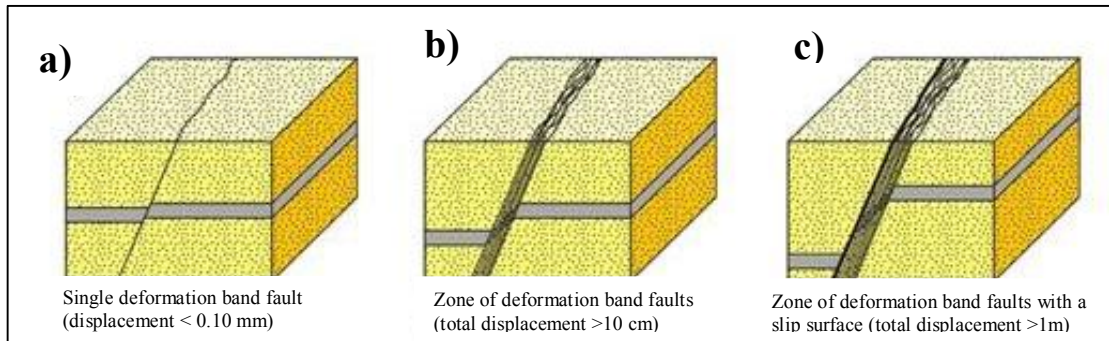


Fig. 1.3. Sketch showing a single deformation band (a), and a zone of deformation bands with slip surfaces (b & c).
<http://www.ig.tuwien.ac.at/forschung/schwerpunkte/deformation-mechanism-in-porous-sediments.html>.

1.1.3. Comparison with ordinary faults

There are several important characteristics that distinguish deformation bands from ordinary fractures (such as slip surfaces or extension fractures):

- a. They are thicker and exhibit smaller offsets than classical slip surfaces of comparable length (Fig. 1.3c).
- b. Where cohesion is lost or reduced across ordinary fractures, most deformation bands maintain or even increase cohesion.
- c. Deformation bands often exhibit a reduction in porosity and permeability, whereas, both slip surfaces (faults) and tension fractures (veins) are typically associated with a permeability and porosity increase.
- d. Strain hardening behaviour, commonly associated with deformation band formation, also contrasts to the strain softening associated with classical fractures.

1.2. Purpose of investigation

The purpose of this study is to understand the orientation, kinematics and sequential development and evolution of deformation bands by using numerical modeling approach. Though, deformation bands have extensively been studied in the field (Davis et al., 1999) and their formation has been investigated through physical experiments (Schultz and Siddharthan, 2005); this study will focus on the formation mechanism of deformation bands using finite difference code.

For this reason, a sandstone sample having well developed deformation bands was collected from the Dhok Pathan Formation exposed in the Qabul Khel area (Long. $71^{\circ}08'27.45''$ and Lat. $32^{\circ}39'10.8''$), which is located at the southern tip of the Surghar-Shinghar Range, north Pakistan (Fig. 1.4). In this area, excellent exposures of deformation bands in sandstone of the Dhok Pathan Formation of Pliocene age have been reported (Sayab et al., 1999). It has been envisaged that the formation of the

deformation bands in the Qabul Khel area are linked to the Surghar Thrust (Sayab et al., 1999).

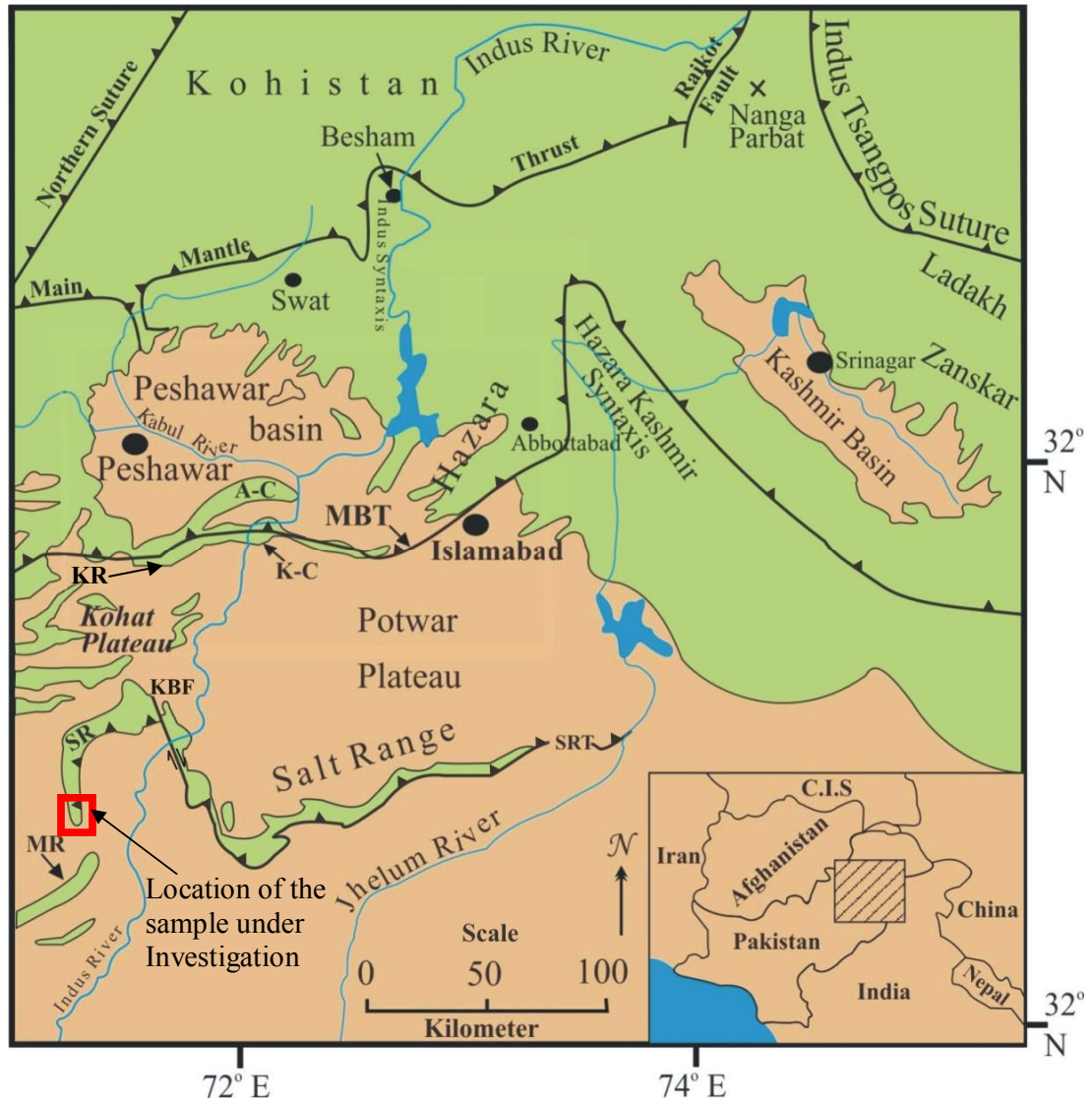


Fig. 1.4. Location map of the Himalaya of north Pakistan and northwestern India showing the major faults and mountain ranges (Baker et al. 1988). Dark red square in the figure represents the sampling area.

A-C=Attock-Cherat Range; K-C=Kalachitta Range; SR=Surghar-Shinghar Range; MR=Marwat Range; MBT=Main Boundary Thrust; SRT=Salt Range Thrust, BB=Bannu Basin; KR=Kohat Range.

1.3. Numerical modeling

Numerical modeling is a powerful empirical technique that has recently been introduced and extensively used to understand the geological processes (McLellan et al., 2004; Fay et al., 2008; Johnson, 2009; Uzkeda et al., 2010). The advantage of this technique over other modeling techniques is that it allows user to model any particular physical/geological phenomenon and associated problem in various steps that follow sets of executable commands based on mathematical equations. The executable commands are written in a meaningful semantics that lead to answerable simulation. The results can be directly comparable to given physical process/problem at any stage with an advantage of quantitative outputs. It allows a detailed investigation of the deformation and stress distribution inside the system being able to reveal quite complex mixture of tensile, compressive, shearing and bending forces (Shimizu et al., 2004).

To perform numerical simulations, controlled experiments and variety of different constitutive modeling codes are used. Since 1980, Itasca Inc., an international engineering consulting and software development firm, has pioneered the use and development of numerical modeling codes for solving hydrogeological and geomechanics related problems in mining, civil, petroleum, process engineering, waste isolation, and environmental industries. It has developed different numerical codes that provide unparalleled speed, power, and proven capability for handling problems related to geomechanics. For this study, I have used finite difference code FLAC-2D (licence courtesy of Dr. Qaiser Iqbal, Assistant Profesor, UET, Peshawar) to model the formation of deformation bands in sandstone.

1.4. Geological setting of the area

The sample and area under consideration forms part of the southern Surghar-Shinghar Range. The Surghar-Shinghar Range constitutes an important geometric component of Trans-Indus Himalayan ranges in the NW Pakistan. The Marwat-Khisor and Pizu- Manzai ranges are other components of Trans-Indus Ranges. These ranges are the western continuation of the Salt Range (Gee, 1989), displaced from the Salt Range by the Kalabagh Fault (Yeats et al., 1984; Fig. 1.4). Surghar-Shinghar Range is an arcuate mountain belt, forming the southeastern proximity of the Kohat plateau. It has east-west orientation switching to a north-south trend while bordering the eastern flank of the Bannu Basin (Fig. 1.4). The Surghar-Shinghar Range at the eastern margin of the Bannu Basin is a north-south oriented anticline in the hanging wall of the Surghar Thrust (Gee, 1989; Sayab et al., 2001a; Sayab et al., 2001b).

The Surghar-Shinghar Range represents the leading deformational front of the Kohat fold and thrust-belt and is the southernmost surface expression of tectonic uplift associated with the Himalayan Orogeny (Fig. 1.4). Towards north, the Kohat plateau separates it from Kohat Range and towards west the flat lying Bannu Basin separates it from the northern Sulaiman Range (Fig. 1.4). Regional strike of the Surghar-Shinghar Range from Qabul Khel to Thatti- Nasrati is north-south, dipping towards west with an angle of about 45° - 50° at the outer limbs to the core of the anticline (Sayab et al., 1999).

The north-south trending part of the Surghar-Shinghar Range is divisible into two anticlines, Makarwal anticline (Danilchik and Shah, 1987) to the north and Sarkai-Mochi Mar (SMM) anticline to the south (Sayab et al., 2001a). The eastern flanks of these anticlines are deeply eroded to form steep scraps, exposing core formations, which are uplifted, over-folded and characterize the surface trace of the

Surghar Thrust (Gee, 1989; Danilchik and Shah, 1987; Sayab et al., 2001b). The southern tip of the SMM anticline host excellent exposures of deformation bands in sandstones. The deformation bands form ‘conjugate’ and complex ‘Riedel’ geometries. In this study, attempt is made to model these geometries using numerical modeling approach.

1.5. Stratigraphy of the Surghar-Shinghar Range

General stratigraphic setup of the Surghar-Shinghar Range is tabulated in

Table 1.1.

System	Proposed Stratigraphy of Surghar-Shinghar Range
TERTIARY & QUATERNARY	Sub-Himalayan super-Group (in parts) Siwalik Group { Dhok Pathan Formation Nagri Formation Chinji Formation
TERTIARY	Mitha Khattak Formation Sakesar Limestone Nammal Formation Patala Shale Lockhart Limestone Hangu Formation (include Makarwal coal bed)
CRETACEOUS	Lumshiwali Formation Chichali Formation
JURASSIC	Samana Suk Formation Shinawari Formation Datta Formation
TRIASSIC	Kingriali Formation
	Tredian Formation { Khatkiara Sandstone member Landa member
PERMIAN (UPPER)	Mianwali Formation { Narmia Member Mittiwali Member Kathwai Member
	Zaluch Group { Chidru Formation Wargal Limestone

Table 1.1. Stratigraphy of the Surghar-Shinghar Range (Danilchik and Shah, 1987).

The oldest formations exposed in the Surghar-Shinghar Range are of the Permian Zaluch Group (Wargal Limestone and Chidru Formation) along the Salt Range Thrust or the Surghar Thrust (Gee, 1989). This is followed by Mesozoic-Lower Tertiary sequence comparable to that of the western Salt Range. The Siwalik sequence dominates in the upper part (Table 1.1). The present study deals with the Dhok Pathan Formation of Surghar-Shinghar Range.

1.5.1. Dhok Pathan Formation

Pilgrim (1913) introduced the name 'Dhok Pathan' for fauna collected from interbedded siltstone and sandstone unit constituting the upper part of Middle Siwalik. However Cotter (1933) redefined the unit as the 'Dhok Pathan Formation' and this name has been formalized by the Stratigraphic Committee of Pakistan in 1973. Dhok Pathan village near Soan River on Attock-Talagang road in district Attock is designated as its type section. It has conformable and transitional lower and upper contacts with the Nagri and Soan Formations, respectively. The formation is comprised of deep orange to red color siltstone and grey sandstone with occasional bands of conglomerate.

In Surghar-Shinghar Range the Dhok Pathan Formation shows alternate sedimentary rhythms of shale, siltstone and sandstone units (Azizullah, 1995). The color of sandstone varies from light grey to ash grey and is generally fine-to medium-grained, but within paleochannels, coarse-grained gritty sandstone is also present. The sandstone bodies are friable, cross bedded (Fig. 1.5), poorly cemented except for the hard sandstone bands which make prominent walls because of their resistance against weathering that make them stand out than the adjacent friable sandstone (Fig. 1.6 and 1.7). Shales are generally light reddish brown, whereas siltstone is brown. Thickness

of the formation varies from 950 to 1200m (Azizullah, 1995). Age of the Dhok Pathan formation in the Shinghar Range is 2.7 Ma (Khan and Opdyke 1987).



Fig. 1.5. Photograph showing the sandstone of the Dhok Pathan Formation near Qabul Khel area. The sandstone is coarse grained, moderately sorted, comparatively less compacted and laminated following the cross-bedding.



Fig. 1.6. Photograph showing light grey, massive sandstone of the Dhok Pathan Formation near Qabul Khel area. Here sandstone is coarse grained, highly compacted, occasionally cemented and comparatively well sorted. Hard sandstone bands are frequent in the formation.

1.6. Aims and objectives

The main objectives of the present study are:

- a) To study and characterize the deformation bands using published material models.
- b) To develop a code using established material properties of sandstone and design boundary conditions that help to generate the deformation bands.
- c) To understand the step-by-step tectonic evolution of deformation bands and their geometries.
- d) To see, how the ‘Riedel’ and ‘conjugate’ patterns link with each other during the simulations.
- e) To calculate the stress needed to produce the deformation band geometries in porous sandstone.

1.7. Methodology

A sandstone sample, having distinct sets of deformation bands collected from the Dhok Pathan Formation of Pliocene age, Surghar-Shinghar Range, was selected for this study (Fig. 1.7), and used as a reference to model the deformation bands in porous sandstones. Finite difference code of Itasca Inc. (FLAC-2D) was used to numerically simulate the structural evolution of deformation bands in sandstones. To generate model steps, FLAC-2D requires mechanical properties of porous sandstone that is an essential ingredient of the data file for execution. In this regard, the mechanical properties of porous sandstones are very carefully taken from the literature and used for the modeling purposes (e.g. Okubo and Schultz, 2005; Fig. 1.8).

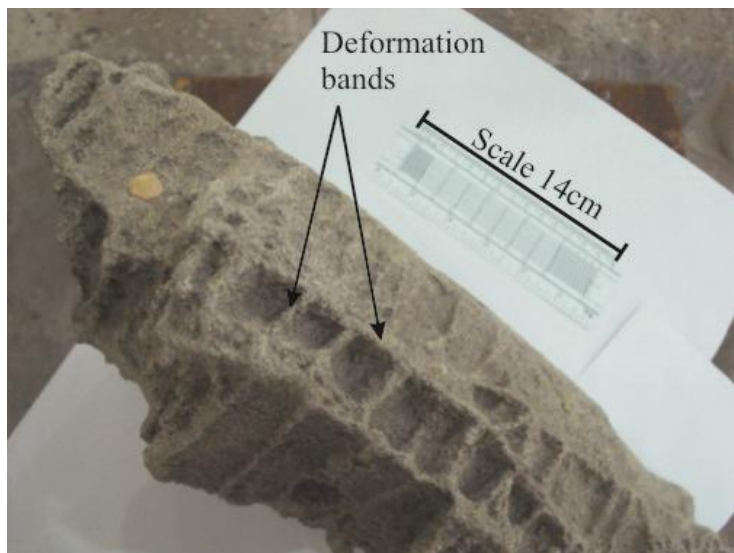


Fig. 1.7. Deformation bands in porous sandstone from the Dhok Pathan Formation, Surghar-Shinghar Range. In the field, they either form 'conjugate' geometry or 'Riedel' pattern.

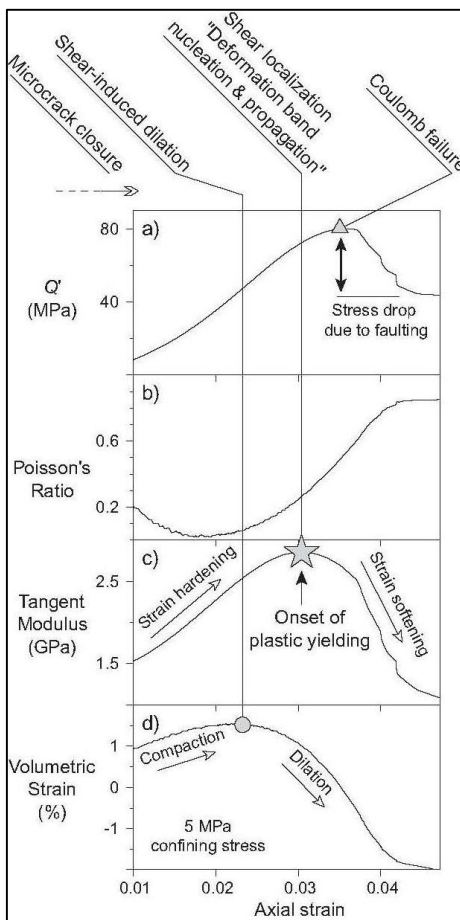


Fig. 1.8. Triaxial compression results of sandstone (after Okubo and Schultz, 2005).

1.7.1. Mechanical properties of material

Brief description of the key properties of material incorporated in the data file is given below:

1. Density (ρ)

The density can be defined as mass per unit volume of the material under consideration, and expressed in mass per unit volume (e.g. kg/m^3).

2. Bulk modulus (K)

Bulk modulus is defined as pressure required to cause a relative decrease in volume of a substance and is represented in pascal (Pa).

3. Shear modulus (G)

It is defined as the ratio of shear stress to the shear strain and is measured in gigapascals (GPa) or thousands of pounds per square inch (ksi).

4. Angle of internal friction (θ)

It is the angle on the graph (Mohr's Circle) of the shear stress and normal effective stresses at which shear failure occurs. Angle of internal friction can be determined in the laboratory by the Direct Shear Test or the Triaxial Stress Test.

5. Tensile strength (TS)

Tensile strength (TS) is the measure of maximum stress that a material can withstand while being stretched or pulled before necking. The tensile strength is usually calculated by performing tensile test and recording the stress versus strain curve in which the highest point is the tensile strength. It is the opposite of compressive strength and is measured as force per unit area. In the SI system, the TS is expressed in pascal (Pa) or newtons per square metre (N/m^2).

6. **Dilation angle (ψ)**

The dilation angle (ψ) is the change in the orientation of grains on a shearing surface. This angle is related to the angle of internal shearing resistance i.e. friction angle. Clays are characterized by a very low amount of dilation i.e. $\psi=0$ while for sands, the angle of dilation depends on the angle of internal friction.

7. **Cohesion (c)**

Cohesion is the force that holds together molecules or like particles within a material. It is the component of shear strength of a rock or soil that is independent of inter-particle friction and measured in pascals (Pa). Cohesion is usually determined in the laboratory from the Direct Shear Test. Cohesion is caused by one of the following components:

1. Electrostatic forces in stiff over-consolidated materials which may be lost by weathering.
2. Cementing by Fe_2O_3 , CaCO_3 , NaCl etc.
3. Negative capillary pressure (which is lost upon wetting).
4. Pore pressure response during undrained loading (which is lost through time).

1.7.2. **FLAC-2D: data file and execution**

Following are the steps, which were followed in creating the numerical model of the proposed problem.

- a) Data file consist of set of executable commands (e.g. generate mesh, assign material model properties, boundary and initial conditions).
- b) Secondly, data file was imported in the FLAC-2D program that solved the commands to bring the system in equilibrium.
- c) Model was allowed to run in large/small strain mode for calculations in steps.

- d) The experiment was run to a total extension of 100% so that the deformed grid could easily be compared to the problem geometry.

1.8. Significance

The study of deformation bands is important in many ways. For example, they provide important information on the process of faulting in porous media and have direct implications for the migration of fluids in hydrocarbon and groundwater reservoirs in which they are very likely to occur (Fossen et al., 2007).

The results of this study are novel to understand the step-by-step tectonic evolution of deformation bands using numerical simulations. The results of different experiments eventually helped in developing the suitable parameterizations that can be used to model ‘conjugate’ and ‘Riedel’ geometries. In addition, results are able to predict the density of stress and strain energy distributed in the model. This indicates that the numerical modeling is a powerful approach that can quantify the geological processes in terms of tectonic forces and answer many questions in this regard.

CHAPTER - 2

'CONJUGATE' AND 'RIEDEL' DEFORMATION BAND PATTERNS

CHAPTER 2

'CONJUGATE' AND 'RIEDEL' DEFORMATION BAND PATTERNS

2.1. Introduction

Deformation bands (Aydin, 1978; Antonellini et al., 1994) are planar to curvilinear continuous structures of small offset of few mm to few cm characterized by localized shear and porosity change. These zones of localized deformation, in most cases, are mechanically stronger and with lower porosity than surrounding rocks (Aydin et al., 2006; Fossen et al., 2007). Material produced in deformation band zone has a much smaller grain size and poor sorting than the original sandstone. They can restrict and/or change the flow of fluids like oil and water.

In porous sandstones, deformation bands commonly occur as either 'conjugate' or 'Riedel' pattern geometry. Intersecting shear fractures that have opposite senses of slip are called 'conjugate' fractures in the literature (Davis et al., 1999). Ideal 'conjugate' fracture pairs have an acute angle (roughly 60°) that is bisected by the maximum compressive stress at the time of fracturing (Anderson, 1942; Fig. 2.1). Whereas the term 'Riedel' refers to a specific geometry or fault pattern first created in clay cake models (Riedel, 1929), which exhibits relatively short, en echelon fracture segments of synthetic R and antithetic R' shears oriented at low- and high- angles to the main strike-slip fault zone, respectively (Antonellini et al., 1994; Davis et al., 1999) (Fig. 2.1b and 2.2). The complete 'Riedel' pattern may consist of a series of five elements oriented at specific angles to the trend of Principal Shear Zone (PSZ) (Fig 2.3). These elements include:

1. 'Conjugate' R and R' fractures in right-lateral PSZ formed at $+15^\circ$ and $+75^\circ$ degrees, respectively,
2. P shears (inclined at -15 degrees) in the same shear regime,
3. T fracture (inclined at 45°),
4. Y shears (oriented sub-parallel/parallel to the trend of PSZ and also called as Principal Displacement Shears).

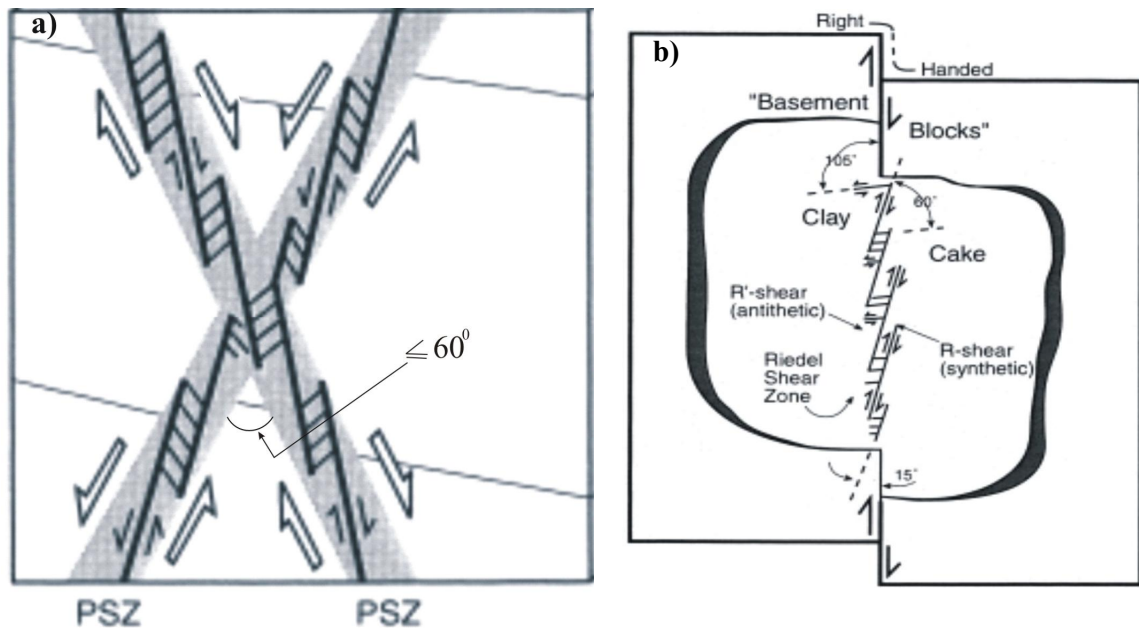


Fig. 2.1. (a) Block diagram showing the fundamental geometric relations of the 'conjugate' deformation bands and 'Riedel' systems, and (b) map view of the 'Riedel' shear zone formed in a clay cake model (after Davis et al., 1999).

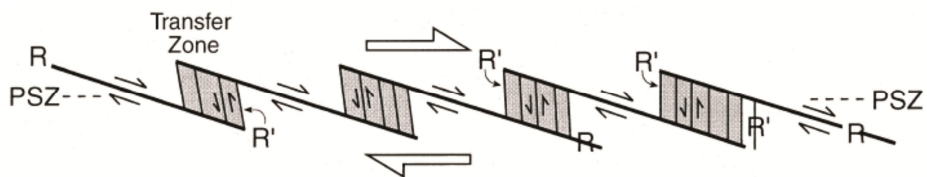


Fig. 2.2. Schematic sketch showing a 'Riedel' shear zone composed of R and R' shears linked by transfer zone (after Davis et al., 1999).

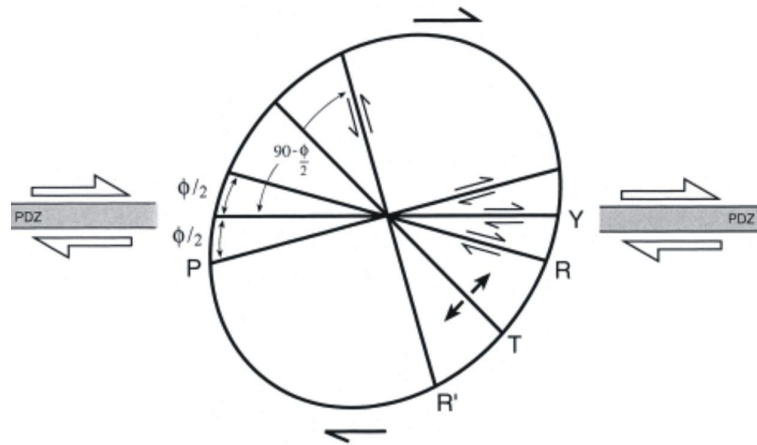


Fig. 2.3. Drawing of the common elements within an ideal ‘Riedel’ shear system (after Bartlett et al., 1981; Woodcock and Schubert, 1994).

2.2. Mechanism of the formation of deformation bands

Aydin (1978) and Aydin and Johnson (1978, 1983) concluded that individual deformation bands most commonly form as a result of a transpressional shearing involving the shear-induced collapse of pore spaces; translation and rotation of quartz grains into direct contact; grain-contact and stress build-up that causes grain-scale micro fracturing; and grain-size reduction through continued shear-induced cataclastic flow (Fig. 2.4). There are some other varieties of deformation bands and deformation band mechanisms than those described above (Antonellini et al., 1994a; Davis et al., 1999). Some deformation bands may form during primary deposition, compaction, and gravitational loading of aeolian sands through mechanisms dominated by granular flow and the development of ‘conjugate’ normal shear zones lacking signs of cataclastic flow and tectonic deformation (Davis et al., 1999). Others are analogous to cleavage, forming perpendicular to the direction of greatest contraction and reflecting volume loss but no shear (Mollema and Antonellini, 1996). Some deformation bands

may also form by phyllo-silicate smearing, dissolution and cementation process (Antonellini et al., 1992).

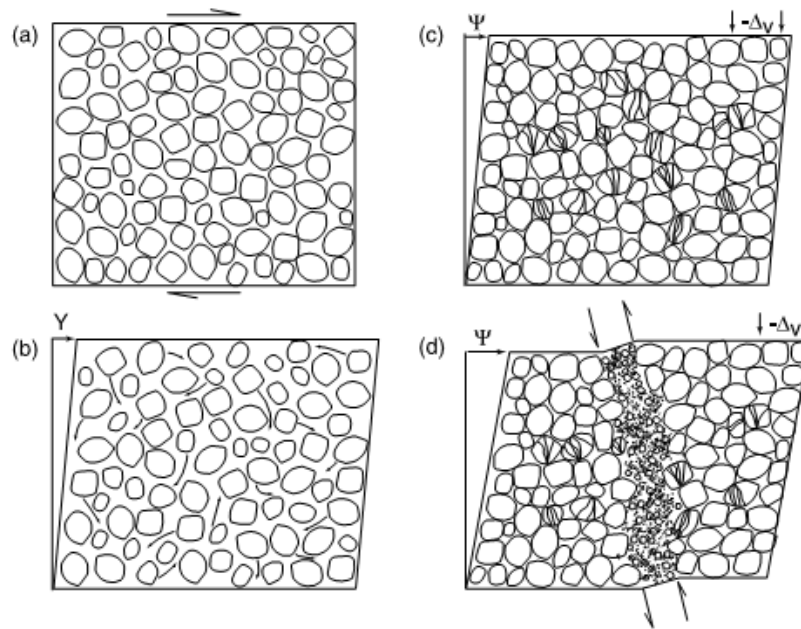


Fig. 2.4. Idealized sequential development of deformation band zone in porous sandstone. (a) Undeformed fluid saturated sandstone is subjected to dextral shearing. (b) Elevated pore fluid pressure results in positive dilation, which causes increase in porosity during shearing. (c) Continued shearing results in grain crushing and incipient cataclasis. (d) Cataclastic deformation, pore spaces collapsed, yielding localized shear bands 1-2 grains wide (after Lucas and Moore., 1986).

Deformation bands of tectonic origin form in highly porous sandstones ($\pm 25\%$ porosity). They are fault-like features in that they accommodate shear displacement and thus cause offset of markers, such as cross-bedding (Fig. 1.3). However, the physical properties of deformation bands are generally not fault-like, as the mechanism is not one of strike-slip deformation and also don't represent the development of a discrete fracture surface (Byerlee and Brace, 1968) (Fig. 1.2). At the

site of a zone of deformation bands the volume loss is considerably enormous. For example, a host rock porosity of more than 20% may be reduced to less than 1% (Antonellini and Aydin, 1994). Deformation bands, therefore, don't look like faults. Instead, they are very thin (mm-scale) to thick (cm- to m-scale) shear zones that resemble quartz veins or quartz lodes, which are resistant to weathering and erosion.

2.2.1. Controlling factors of the deformation bands

A number of factors, including confining pressure (burial depth), deviatoric stress (tectonic environment), pore fluid pressure and host rock properties, such as degree of lithification, mineralogy, grain size, sorting, and grain shape controls the formation of deformation bands (Fossen et al., 2007).

2.3. Previous work

Since the pioneering work of Riedel (1929), understanding the evolution of deformation bands in porous rocks is still an attractive subject in the literature (Fossen et al., 2007; Rotevatn et al., 2009). Considerable amount of theoretical work on the development of deformation bands has been carried out (Fossen et al., 2007). Numerous workers have described the deformation bands, their mechanism of formation, nucleation and evolution in porous sandstone (Cloos, 1955; Aydin, 1978; Aydin and Johnson., 1983; Antonellini et al., 1994 and Ahlgren, 2001). 'Conjugate' systems of deformation bands have been observed and described in the field by number of workers like Antonellini et al. (1994), Garcia and Davis (1997); Davis et al. (1999) and Olsson et al. (2004) and in the laboratory by Friedman and Logan (1973), Mair et al. (2000), and Olsson (2000). 'Riedel' pattern in sandstone has also been documented in many studies (Davis, 1996; Davis et al., 1999; Ahlgren, 2001);

Fossen et al., 2007). Computer simulation of shear bands formation in frictional-dilational material was also carried out by Hobbs and Ord (1989) to measure the inclination of individual shear bands with the principal axis of compression.

However, the sequential development of deformation bands within a ‘conjugate’ or ‘Riedel’ system scheme is poorly understood (Fossen et al., 2007). Therefore, in this study, numerical modeling approach was adopted to simulate nucleation and growth of deformation bands in ‘conjugate’ and/or ‘Riedel’ geometries in sandstone using field examples of Dhok Pathan sandstone as a reference (Fig. 2.5).



Fig. 2.5. Photograph showing NW-SE trending shear zone and associated ‘Riedel’ deformation bands from the Dhok Pathan Formation of the Surghar-Shinghar Range (Photo after Kamran, Ahmad and Islam., 2006).

CHAPTER - 3

NUMERICAL SIMULATION OF DEFORMATION BANDS

CHAPTER 3

NUMERICAL SIMULATION OF DEFORMATION BANDS

3.1. Introduction

Numerical modeling is a powerful empirical technique to investigate the natural geological phenomena in commercially available software. The significance of the numerical modeling technique over other methods is that it uses the established material model codes for rocks and produce results based on pre-defined set of mathematical equations. This study shows how different steps have been taken to closely model the ‘conjugate’ and associated ‘Riedel’ pattern that naturally formed in sandstones. Finite difference code, FLAC-2D was used to model the proposed geometry.

3.2. FLAC-2D

3.2.1. Introduction

FLAC-2D (Fast Lagrangian Analysis of Continua) is a two-dimensional explicit finite difference program and extensively been used for rock mechanics (Hobbs and Odd, 1989) and engineering mechanics computation. FLAC-2D was first developed by Dr. Peter Cundall in 1986 specifically to perform engineering analyses on an IBM-compatible micro-computer. This software preferably uses the explicit finite difference scheme to find the numerical solutions of time-dependent systems. FLAC-2D simulates the behavior of structures built of soil, rock or other materials that may undergo plastic flow when their yield limits are reached. Materials are represented by elements or zones, which form a grid that is adjusted by the user to fit the shape of the object to be modeled. Each element behaves according to a

prescribed linear or nonlinear stress or strain law in response to the applied forces or boundary conditions. The material can yield and flow and the grid can deform (in large-strain mode only) and move with the material that is represented. The explicit Lagrangian calculation scheme and the mixed-discretization scheme (Marti and Cundall, 1982) used in FLAC ensure that plastic collapse and flow are modeled very accurately. Because no matrices are formed, therefore large two-dimensional calculations can be made without excessive memory requirements.

3.2.2. Material models

Several built-in constitutive models that permit the simulation of highly nonlinear, irreversible response representative of geologic or similar materials are available in the FLAC. There are eleven built-in material models in FLAC and each model is developed to represent a specific type of constitutive behavior commonly associated with geologic materials:

1. Null model (this model is used to represent the material that is removed or excavated).
2. Elastic, isotropic model
3. Elastic, transversely isotropic model
4. Drucker-Prager plasticity model
5. Mohr-Coulomb model
6. Ubiquitous-joint model
7. Strain-hardening/softening model
8. Bilinear strain-hardening/softening ubiquitous-joint model
9. Double-yield model
10. Modified Cam-clay model, and
11. Hoek-Brown plasticity model.

In addition, to these constitutive models, FLAC contains many other special features that can be used in simulation of the real-physical problem(s). FLAC also contains the powerful built-in programming language FISH (short for FLACish) with which one can write his/her own functions to extend FLAC's usefulness, and even implement his own constitutive models, if required.

3.2.3. FLAC-2D operation

FLAC can be operated as either a menu-driven or a command-driven computer program. The menu-driven mode provides easy-to-use mouse access to FLAC operation by generating and applying all the input required for a FLAC simulation, in response to point-and-click operations. However, the command-driven mode requires knowledge of the word-command 'language' used by FLAC programme. FLAC can then be run in command-driven mode, either interactively (i.e., entering FLAC commands in the FLAC environment) or from an input data file. The data file (.dat) may be created and modified by the user using any text editor and it contains the set of FLAC commands that represent the problem under consideration. Several data files can be linked to run a number of FLAC analyses in sequence. There are over 40 main commands and nearly 400 command modifiers which are recognized by FLAC.

The software is designed for high-speed computation of models containing several thousand elements. For example, FLAC can solve a model containing up to 30,000 elements of Mohr-Coulomb material on a microcomputer with 24MB RAM. The solution speed for a model of this size is roughly 14 calculation steps per second on a 2.4 GHz Pentium processor. The speed is essentially a linear function of the number of elements; a model of 15,000 elements would require half the runtime to process the same number of calculation steps.

3.2.4. FLAC applications

FLAC was developed primarily for geotechnical engineering applications but now it is widely used in the fields of mining, petroleum, underground engineering, earthquake engineering, civil engineering, rock mechanics, process of localization and evolution of shear bands in frictional materials, ground water flow logic and coupled mechanical-fluid flow analysis, nuclear engineering, and environmental sciences. The basic formulation for FLAC is for a two-dimensional plane-strain model having a wide range of capabilities to solve complex problems in geomechanics.

3.3. Numerical modeling of the ‘conjugate’ and ‘Riedel’ deformation bands

In order to produce the deformation bands in porous sandstone, a total of 49 experiments were performed by selecting the homogeneous specimen of mesh representing the original sandstone rock sample. However, only 10 experiments are discussed below. A relatively simple material model (Mohr-Coulomb) with variable boundary conditions was adopted from the available material models in the FLAC. To generate model steps, FLAC programme requires mechanical properties of material that is an essential ingredient of the data file for execution. In this regard, the mechanical properties of sandstone (listed below) are very carefully taken from the literature and used in the data file (e.g. Okubo and Schultz, 2005).

1. Density (ρ): $2.65 \times 10^3 \text{ kg/m}^3$
2. Bulk modulus (K): $2.68 \times 10^{10} \text{ Pa}$
3. Shear modulus (G): $7 \times 10^9 \text{ Pa}$
4. Friction (ϕ): 35°
5. Tensile strength (ts): $1 \times 10^5 \text{ Newton's/m}^2$
6. Dilation angle (ψ): $7^\circ - 10^\circ$
7. Cohesion (c): $1 \times 10^6 - 1 \times 10^{10} \text{ Pa}$

Different plots e.g. velocity vector plot, displacement vector plot, shear strain increment plot and x- and y-components of the instantaneous velocity and displacement were obtained for interpretation, as these contour plots more clearly delineate the orientation and extent of the deformation bands than the distorted mesh/grid at low strains. Although distorted grid plots were also taken into account at a high strain. The unit of velocity everywhere is initial zone length per time setup. The series of numerical experiments on the sandstone sample are listed below.

3.4. Experiment 1:

In order to generate the ‘conjugate’ or ‘Riedel’ deformation band geometry, a finite difference mesh of 2x1 m size was selected. Lateral shear at the top and bottom of mesh using the velocity parameters was applied to develop distinct sets of ‘Riedel’ pattern.

3.4.1. Mesh size and boundary conditions

Mesh size and boundary conditions used in this experiment for modeling the ‘Riedel’ pattern consists of:

1. Mesh size: 250x100 (2x1 m)
2. Velocity: 5×10^{-8} m/steps
3. Confining pressure: 200×10^3 Pa
4. Shear stresses: 200×10^3 Pa
5. Steps: 20,000

3.4.2. Material properties:

Following material properties were selected for the finite difference mesh that represents porous sandstone (Table 3.1).

S.No	Material properties	
1.	Density (ρ)	$2 \times 10^3 \text{ kg/m}^3$
2.	Bulk modulus (K)	$26 \times 10^8 \text{ Pa}$
3.	Shear modulus (G)	$7 \times 10^8 \text{ Pa}$
4.	Friction angle (ϕ)	35°
5.	Tensile strength (ts)	$1 \times 10^{10} \text{ Newton's/m}^2$
6.	Dilation angle (ψ)	5°
7.	Cohesion (c)	$1 \times 10^{10} \text{ Pa}$

Table 3.1. Table showing the material properties used for experiment 1.

3.4.3. Model run

Constant velocity ($5 \times 10^{-8} \text{ m/steps}$) boundary conditions were applied at the top and bottom of the model to a specified number of steps (20,000) to reach the failure state. Pressure of $200 \times 10^3 \text{ Pa}$ was also applied to all sides of the mesh, in order to confine the model. After applying the boundary conditions, model was allowed to run in large strain mode to specified number of steps.

3.4.4. Resultant geometry

Complete model run was closely monitored during the calculations, but at the end no geometries were found in the mesh (Fig.3.1). This is may be due to two reasons:

- a) The applied lateral shear, was not strong enough to deform the mesh,
- b) Mesh size may be large.

Therefore in the next experiment, I changed the velocity variable plus mesh size.

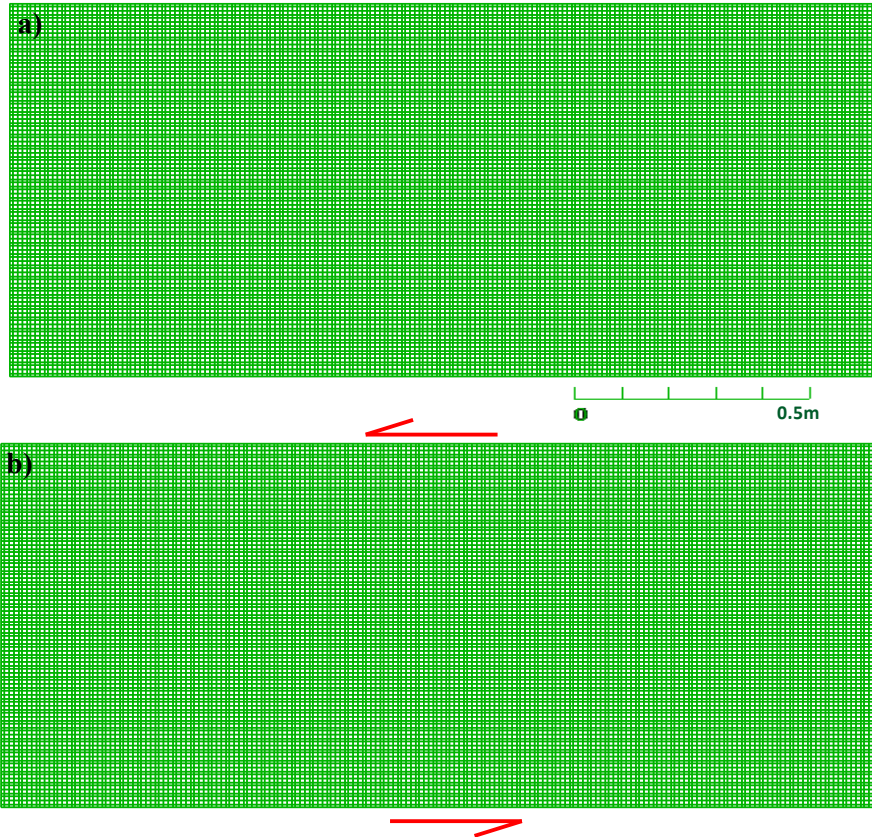


Fig. 3.1. (a) Mesh before applying the boundary conditions, and (b) geometry of the mesh after applying the boundary conditions. Note, no significant change in the mesh.

3.5. Experiment 2:

3.5.1. Mesh size and boundary conditions

After analyzing the length: width ratio of deformation bands in rock sample from the Dhok Pathan Formation, which is 10:2 cm, the mesh size changed accordingly and the velocity boundary conditions were also changed. Mesh size and used boundary conditions are listed below.

1. Mesh size: 200x100 (2x0.3 m)
2. Velocity: 2.5×10^{-7} m/steps
3. Confining pressure: 200×10^3 Pa
4. Shear stresses: 200×10^3 Pa
5. Steps: 20,000

3.5.2. Model run

All other properties were kept constant to that of experiment 1. Model was allowed to run to specified number of steps i.e. 20,000.

3.5.3. Resultant geometry

After completion of calculations, it was observed that, again, no deformation occurred in the mesh (Fig. 3.2 and 3.3).



Fig. 3.2. Mesh before applying the boundary conditions.

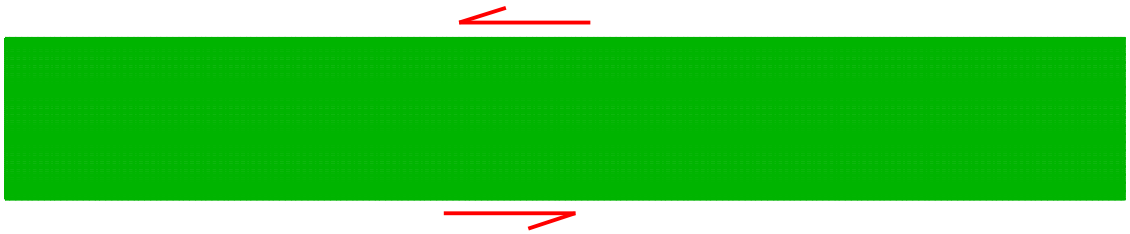


Fig. 3.3. Geometry of the mesh after applying the boundary conditions. Note, no change in the mesh.

3.6. Experiment 3:

After observing the behaviour of the mesh in experiment 2, it was decided further to double the mesh size and changes the velocity boundary conditions from the values used in the previous experiments.

3.6.1. Mesh size and boundary conditions

1. Mesh size: 300×100 (2×0.6 m)
2. Velocity: 2×10^{-8} m/steps
3. Confining pressure: 200×10^3 Pa
4. Shear stresses: 200×10^3 Pa
5. Steps: 50,000

3.6.2. Model run

Model was allowed to run to an extension of 50,000 steps but again stresses and velocity conditions were not strong enough to deform the mesh.

3.6.3. Resultant geometry

Undeformed geometry of the mesh resulted from this experiment as shown in figure 3.4.

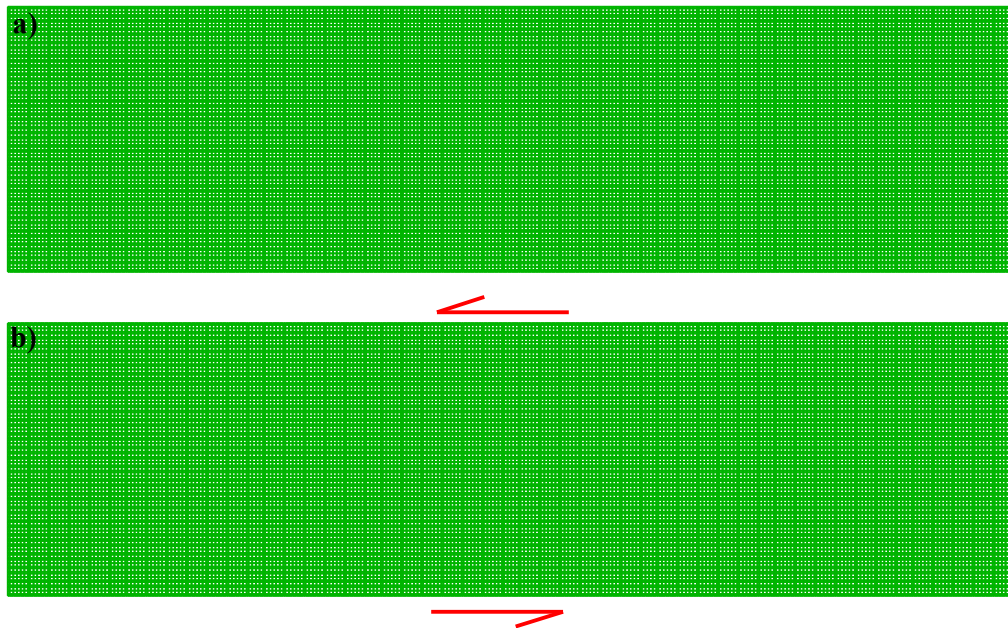


Fig 3.4. (a) Mesh before applying the boundary conditions, (b) mesh remains undeformed after applying the boundary conditions and execution.

3.7. Experiment 4:

For this experiment, average material properties of porous sandstone were first calculated and then incorporated in the data file. Mesh size and velocity conditions were also modified in order to get any possible deformation within the mesh.

3.7.1. Mesh size and boundary conditions

1. Mesh size: 200x150 (2x1.5 m)
2. Velocity: 1.8×10^{-8} m/steps

3. Confining pressure: 200×10^3 Pa
4. Shear stresses: 200×10^3 Pa
5. Steps: 55,000

3.7.2. Material properties

Properties used in this experiment are tabulated below:

S.No	Material properties	
1.	Density (ρ)	2.65×10^3 kg/m ³
2.	Bulk modulus (K)	3.87×10^{10} Pa
3.	Shear modulus (G)	3.96×10^{10} Pa
4.	Friction angle (ϕ)	50.6°
5.	Tensile strength (ts)	4.74×10^6 Newton's/m ²
6.	Dilation angle (ψ)	5°
7.	Cohesion (c)	9.79×10^6 Pa

Table 3.2. Table showing the material properties used for experiment 4.

3.7.3. Model run

After applying the boundary conditions and material parameters to the model, it was allowed to run to an extension of 55,000 steps but at the end, deformation in the mesh was not visible (Fig.3.5).

3.7.4. Resultant geometry

Despite the grid/mesh plot (Fig.3.5), two other plots i.e. displacement vector plot (Fig. 3.6) and velocity vector plot (Fig. 3.7) were also analyzed to confirm the behaviour of velocity and sense of displacement inside the mesh. From all these plots it is noticed that velocity did not penetrate inside the mesh while slipped only at the top and bottom surfaces as shown in fig. 3.6. For this reason there was no visible deformation inside the mesh, though the model was running in large strain mode.

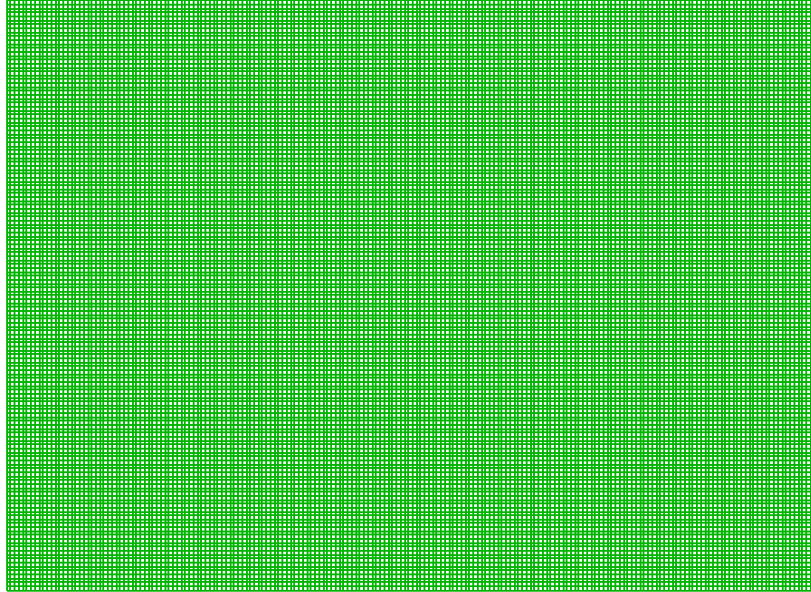


Fig. 3.5. Behaviour of the mesh remains unchanged before and after applying the boundary conditions.

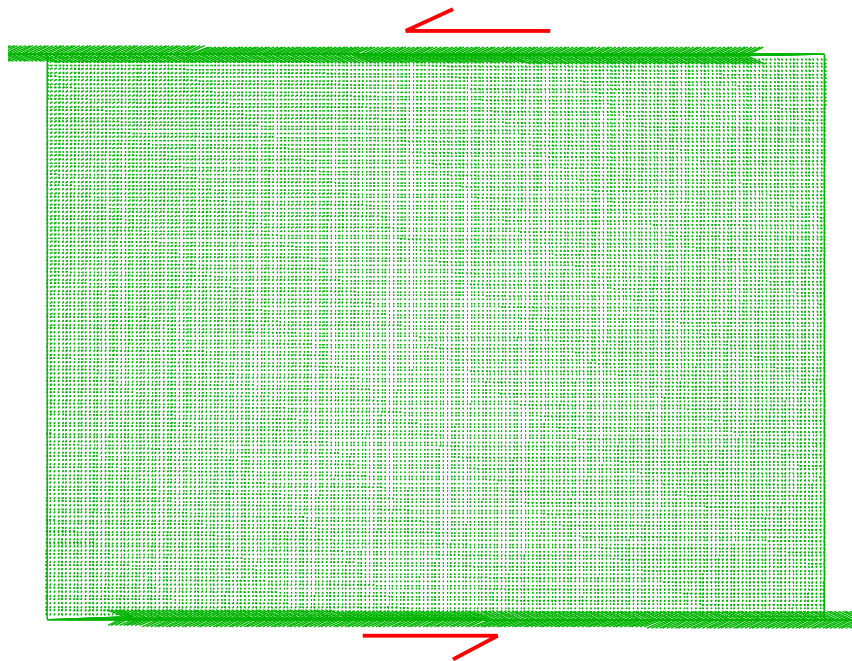


Fig. 3.6. Displacement vectors plot showing the slippage of velocity at the top and bottom surfaces without shearing the internal geometry of the model.

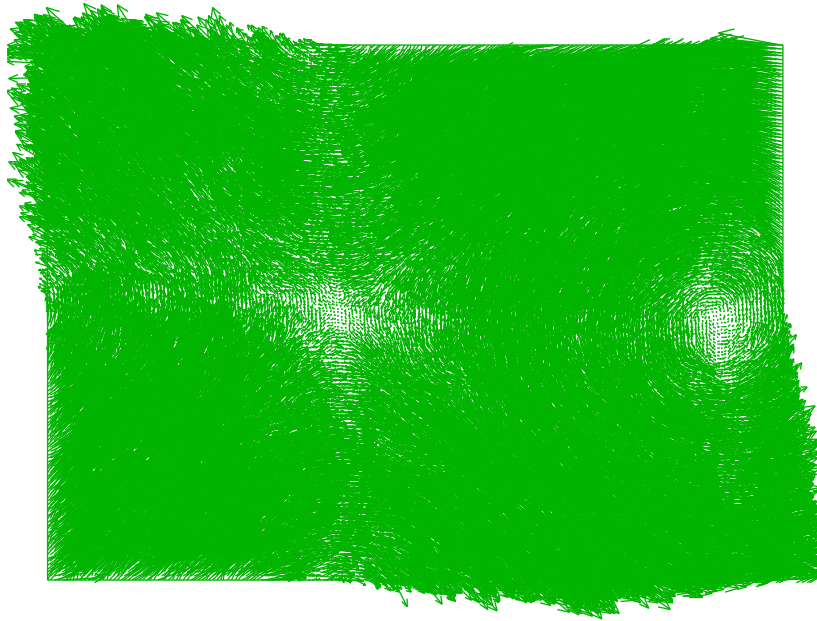


Fig. 3.7. Velocity vectors plot showing little variation of velocity.

3.8. Experiment 5:

For this experiment, I measured the actual dimensions of referred rock sample (Fig. 1.7) and designed the mesh size accordingly.

3.8.1. Mesh size and boundary conditions

1. Mesh size: 250x50 (0.15x0.025 m)
2. Velocity: 5.3×10^{-7} m/steps
3. Confining pressure: 200×10^6 Pa
4. Shear stresses: 200×10^6 Pa
5. Steps: 1,00,000

3.8.2. Material properties

Following material properties were incorporated in the data file for execution:

S.No	Material properties	
1.	Density (ρ)	$2.65 \times 10^3 \text{ kg/m}^3$
2.	Bulk modulus (K)	$2.68 \times 10^{10} \text{ Pa}$
3.	Shear modulus (G)	$7 \times 10^9 \text{ Pa}$
4.	Friction angle (ϕ)	35°
5.	Tensile strength (ts)	$1 \times 10^5 \text{ Newton's/m}^2$
6.	Dilation angle (ψ)	5°
7.	Cohesion (c)	$1 \times 10^6 \text{ Pa}$

Table 3.3. Table showing the material properties used in experiment 5.

3.8.3. Model run

In this experiment, variation command ‘VAR’ was also incorporated in the data file. This command is used in the FLAC programme in order to force the velocities or applied stresses to vary and distribute linearly all inside the model from top to bottom and from left to right. Model was allowed for calculations to 1, 00,000 steps but, again, not successful (Fig. 3.8 and 3.9).

3.8.4. Resultant geometry

The results of experiment 5 are shown below (Fig. 3.8 and 3.9). Besides, testing the lateral shear on sandstone mesh using different mesh size(s) and boundary conditions, no ‘Riedel’ pattern was attained. I asked my supervisor to contact Professor Bruce Hobbs, who is an expert of numerical modeling. We sent him the data file and sketch of our proposed geometry, which we were aiming to produce through numerical simulation. Professor Hobbs very kindly reviewed our data file and executed the file using FLAC. He slightly modified the data file, but no ‘Riedel’ geometry was produced. He then made this comment that ‘Riedel’ geometry may not

produce in lateral shearing. Instead, there may be some other way to produce this geometry (pers. communication through email).

I then radically changed the model to ‘conjugate’ pattern rather than ‘Riedel’ pattern. Therefore, I decided to change the mesh size i.e. mesh representing the outcrop-scale exposures of deformation bands. In addition, instead of applying lateral shearing, load was applied at the top and bottom surface of the model in vertical direction, in order to generate typical ‘conjugate’ geometry.

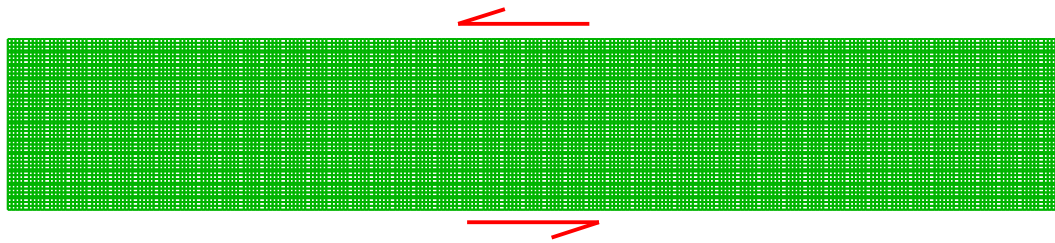


Fig. 3.8. Mesh remains undisturbed though the variation command (VAR) was applied for velocity variations.

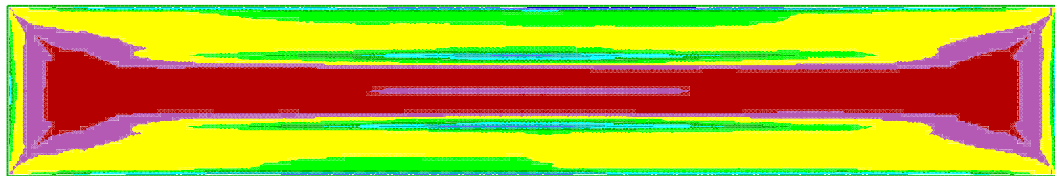


Fig. 3.9. Maximum shear strain increment plot showing the incremental distribution of strain but not enough to deform the mesh.

3.9. Experiment 6:

In this experiment, variable load/force (200×10^2 Pa - 200×10^6 Pa) was applied on top and bottom of the mesh instead of the lateral shear. Mesh size was modified from small- to outcrop-scale, while all other parameters and material properties were kept constant to that of the previous model i.e. experiment 5. To confine the mesh, equal pressure conditions were applied from both left and right side.

3.9.1. Mesh size and boundary conditions

1. Mesh size: 100x100 (100x100 m)
2. Pressure/load: 200×10^2 Pa - 200×10^6 Pa
3. Confining pressure: 200×10^3 Pa
4. Shear stresses: 200×10^6 Pa
5. Steps: 1,02,920

3.9.2. Model run

For this experiment, model was allowed to run for calculations to an extension of 100% without restricting the model to particular number of steps. Model run was completed in 1, 02,920 steps and deformation within the mesh were noticed according to the applied boundary conditions.

3.9.3. Resultant geometry

The output geometry of the mesh used in experiment 6 is shown below (Figs. 3.10 and 3.11). The deformed mesh gives an insight to the development of ‘conjugate’ pattern in the model. All other plots like displacement vectors, velocity vectors and contour plots also represent the strain distribution in the mesh and its deformation.

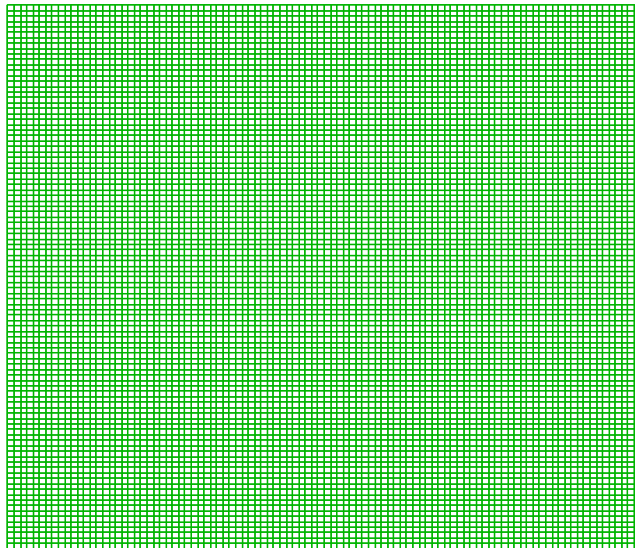


Fig. 3.10. Homogeneous mesh before applying the boundary conditions.

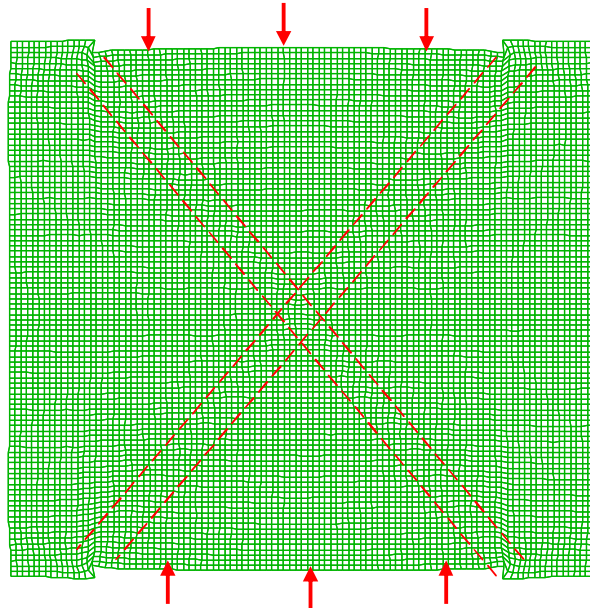


Fig. 3.11. Initial stage of 'conjugate' pattern developed in the homogeneous mesh after applying the boundary conditions and deformation in experiment No. 6.

3.10. Experiment 7:

After getting clues of the development of 'conjugate' deformation bands, from the previous experiment, data file was modified by changing and varying the amount of applied load/force.

3.10.1. Mesh size and boundary conditions

In this experiment mesh size and material properties were kept same to that of experiment no. 6, however only the applied boundary conditions were changed in order to introduce more deformation inside the mesh. In the first test, variable load i.e. 200×10^3 Pa to 200×10^8 Pa was applied at the top and bottom surfaces, while in the second test load varied from 200×10^2 Pa to 200×10^9 Pa at specific sites i.e. top and bottom surfaces.

1. Mesh size: 100×100 (100×100 m)
2. Pressure/load: Variable from 200×10^3 Pa to 200×10^8 Pa, and from 200×10^2 Pa to 200×10^9 Pa.

3. Confining pressure: 200×10^2 Pa to 200×10^3 Pa
4. Shear stresses: 200×10^6 Pa
5. Steps: 100040 and 101339.

3.10.2. Model run

Model completed its run in 100040 and 101339 steps, respectively.

3.10.3. Resultant geometry

As a result of load variation from 200×10^3 Pa to 200×10^8 Pa at the top and bottom surfaces, clear picture of cross-cutting pattern was developed in the mesh (Fig. 3.12). By further varying the load from 200×10^2 Pa to 200×10^9 Pa the ‘conjugate’ pattern became more pronounced (Fig. 3.13).

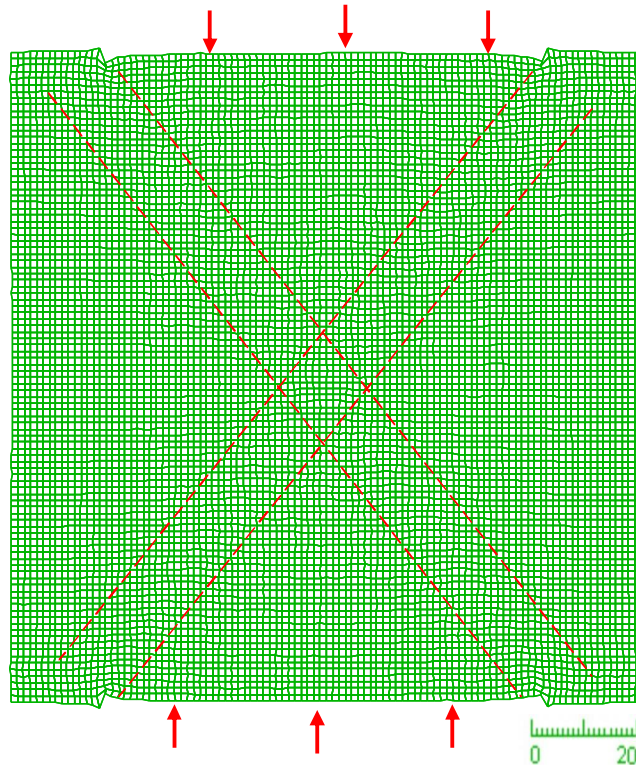


Fig. 3.12. Deformed grid showing the initial stage of the development of cross-cutting sets. Deformation occurs in the mesh by varying load from 200×10^3 Pa to 200×10^8 Pa.

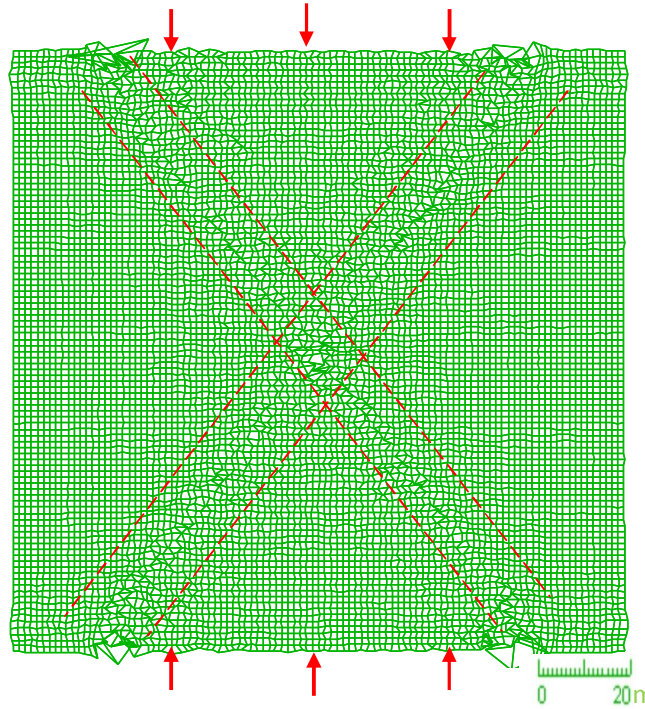


Fig. 3.13. Development of ‘conjugate’ pattern with load from 200×10^2 Pa to 200×10^9 Pa. Note that the deformation bands are not discrete slip surfaces, rather they form zone with ‘continuous’ deformation as proposed in the theoretical models.

3.11. Experiment 8:

In this experiment, dilation angle was increased from 5° to 10° in order to check the effect of this value on the development of deformation bands as proposed by Hobbs and Ord (1989).

3.11.1. Model Run

After the model run up to 100%, it was observed that the formation of ‘conjugate’ pattern is strongly dependent on the value of dilation and friction angles. At a constant value of friction angle, higher value of dilation angle produce pronounced geometry of ‘conjugate’ deformation bands (Fig. 3.14).

3.11.2. Resultant geometry

Model completed in 1, 00,010 steps, with the development of two cross-cutting sets (Fig. 3.14) oriented at an acute angle (to σ_1). Each set consists of a

distinct zone of measureable width. Weak antithetic bands are observed at some places. This antithetic pattern may be the manifestation of R' shear. Several other plots i.e. velocity vectors plot, displacement vectors plot, shear strain increment plot, contour plot and plot showing the distribution of principal stress (described below), were also taken in to account to observe the inside behaviour of the model and to show the 'conjugate' geometry (Fig. 3.15 - 3.18).

a) Velocity vectors plot

Velocity vectors plot shows the distribution of the velocity vectors inside the mesh.

b) Displacement vectors plot

This plot is significant in terms of determining sense of displacement and is consistent with the 'conjugate' shear movement.

c) Shear strain increment plot

Maximum shear strain increment plot shows the strain distribution in mesh and effect of shearing due to applied load.

d) Principal stress plot

This plot is significant in determining the distribution of principal stresses all inside the model.

e) Contour plots

These plots are taken just to see the range of velocity, displacement, displacement in x- and y-direction, and velocity distribution in x- and y-direction. Contour plots normally follow the standard color schemes just to differentiate the value of one range from the other.

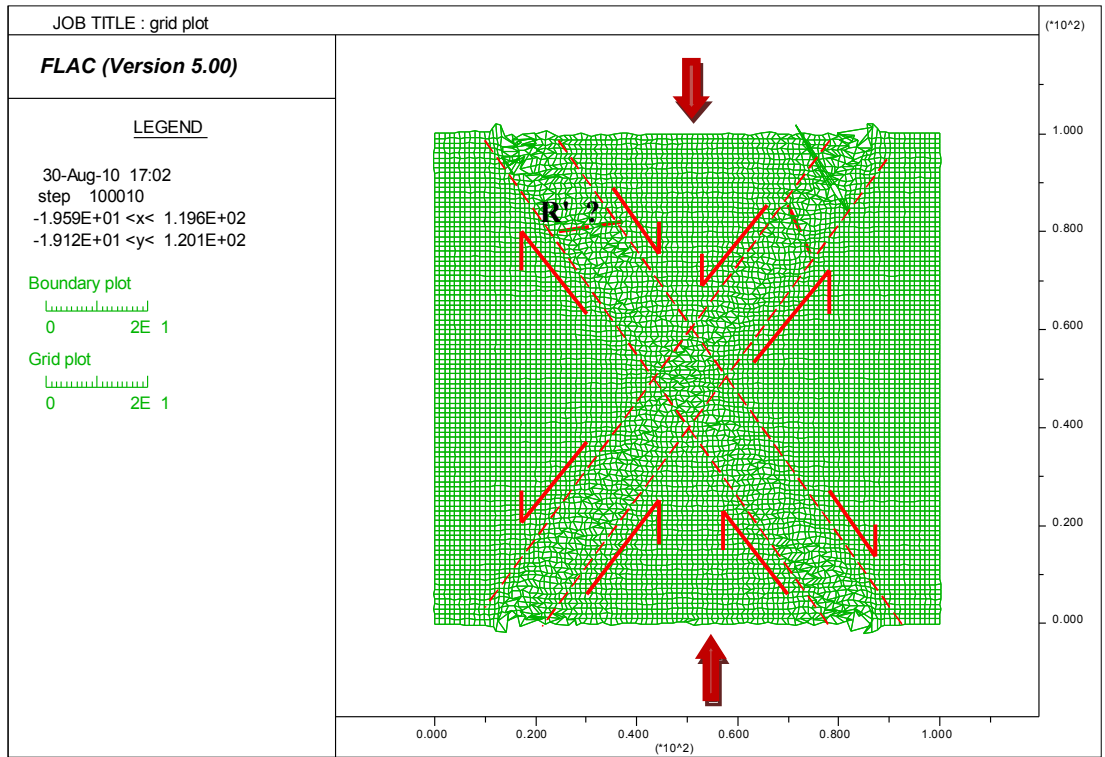


Fig. 3.14. Deformed grid after applying the load and execution. ‘Conjugate’ pattern developed at $\sim 70^\circ$.

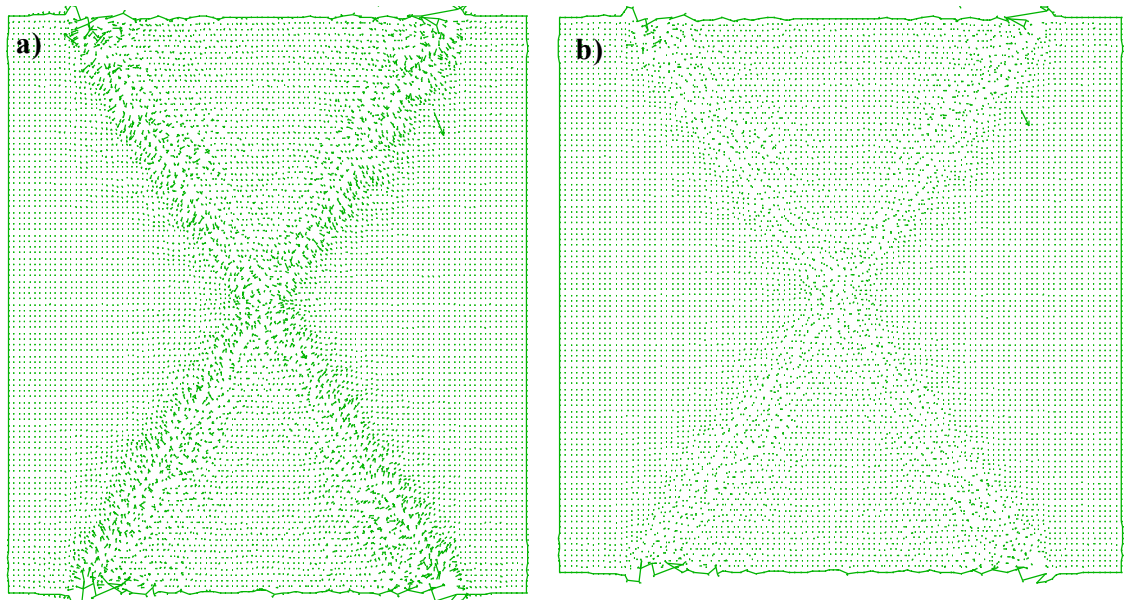


Fig. 3.15. (a) Displacement vectors plot showing the ‘conjugate’ pattern, (b) Velocity vectors plot also showing the ‘conjugate’ pattern and distribution of the velocity vectors inside the mesh.

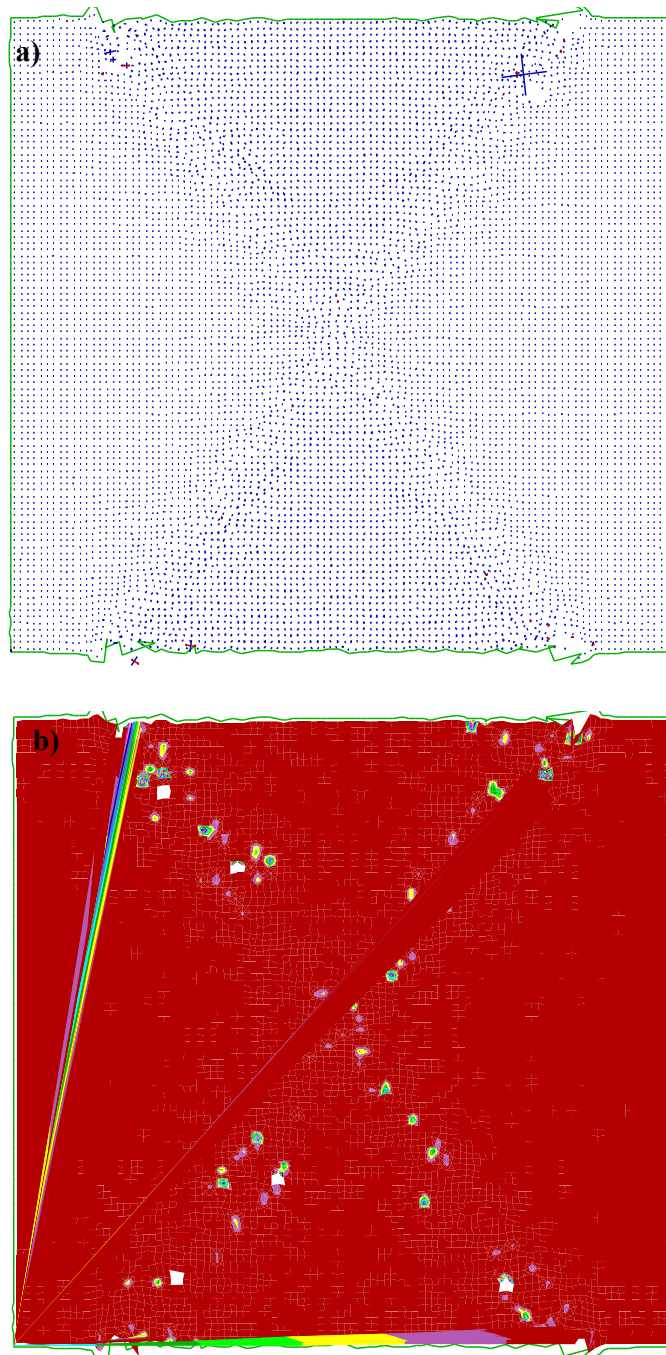


Fig. 3.16. (a) Distribution of principal stresses in the mesh, and (b) shear strain increment plot showing the strain localization.

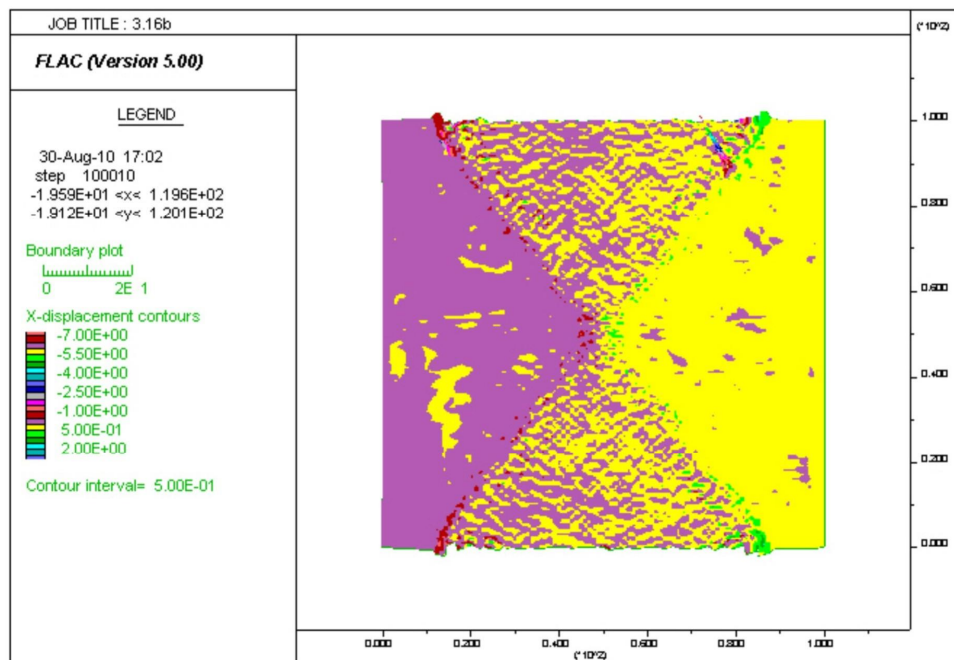
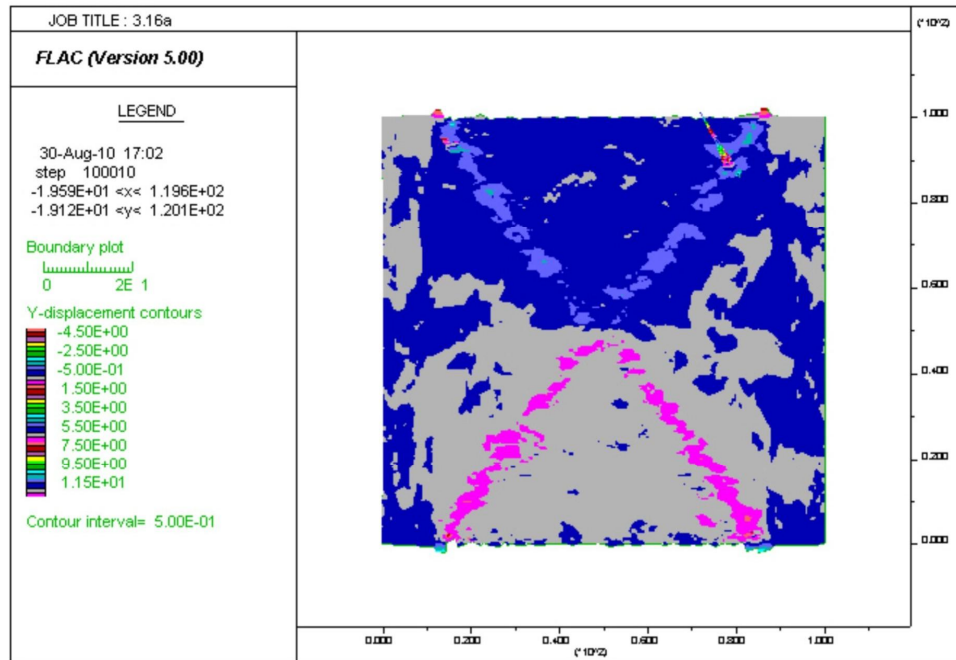


Fig. 3.17. (a) Y-displacement contour plot, contour interval= 5.00×10^{-01} , (b) X-displacement contour plot, contour interval= 5.00×10^{-01} . Both these plots depict the formation of 'conjugate' pattern.

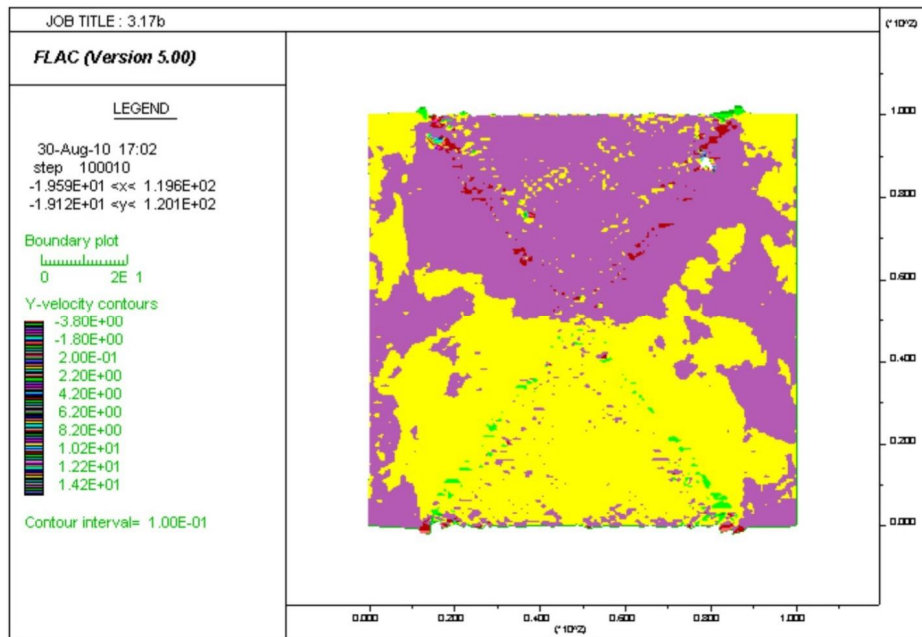
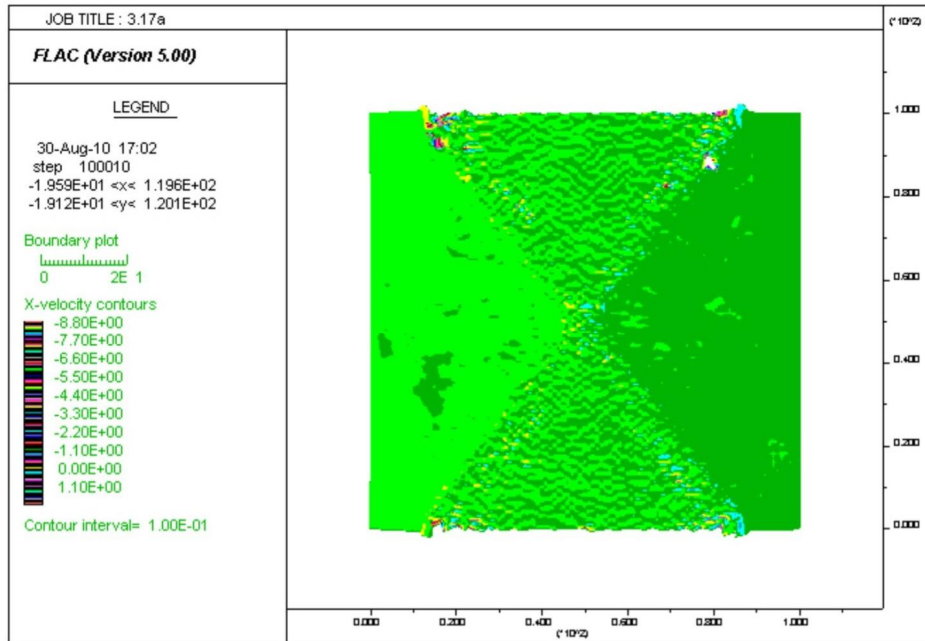


Fig. 3.18. (a) Boundary plot of X-component of velocity, contour interval= 1.00×10^{-01} , and (b) boundary plot of Y-component of velocity, contour interval= 1.00×10^{-01} . These plots also depict the formation of 'conjugate' pattern.

3.12. Experiment 9:

After getting the ‘conjugate’ deformation band geometry, two other experiments were carried out to produce the distinct R' ‘Riedel’ deformation band geometry, as roughly observed in the deformed portion of the ‘conjugate’ sets, in the previous experiment.

3.12.1. Mesh size and boundary conditions

For numerical simulation of ‘Riedel’ deformation bands, mesh size and boundary conditions were selected same to that of experiment 8, in which intersecting ‘conjugate’ geometries were formed.

3.12.2. Material properties

All material properties were same as of experiment 8, except for the value of cohesion, which was relatively higher (1×10^{10} Pa). This will increase the toughness of the sandstone. Usually ‘Riedel’ geometries form in comparatively hard sand, therefore, it was assumed that by increasing the toughness (cohesion), the ‘Riedel’ geometry may be formed. However, after getting the equilibrium condition during the run, the value of cohesion and tensile strength was set to zero, as porous sand is a cohesionless material.

3.12.3. Model run

Model was allowed to run to a total extension of 100% instead of specified number of steps for solution. Small strain mode was selected for this model, as it is assumed in theoretical models that the ‘Riedel’ shears developed in small strain. Model run was completed in 1, 00,010 steps.

3.12.4. Resultant geometry

As small strain mode was selected, therefore, there was no deformation in original mesh. FLAC program allows the mesh to deform only when the model is running in large strain mode, however, the proposed geometry needs to be matched with other plots (e.g. shear strain increment plot, displacement vectors plot, velocity vectors plot, principal stresses distribution plot and contour plots of velocity and displacement). Complete run of model was closely monitored at every step to see the sequential development of deformation bands with main emphasis on the development of 'Riedel' deformation band geometry (R'). The model produced well developed 'conjugate' sets but no R' geometries (Fig. 3.19).

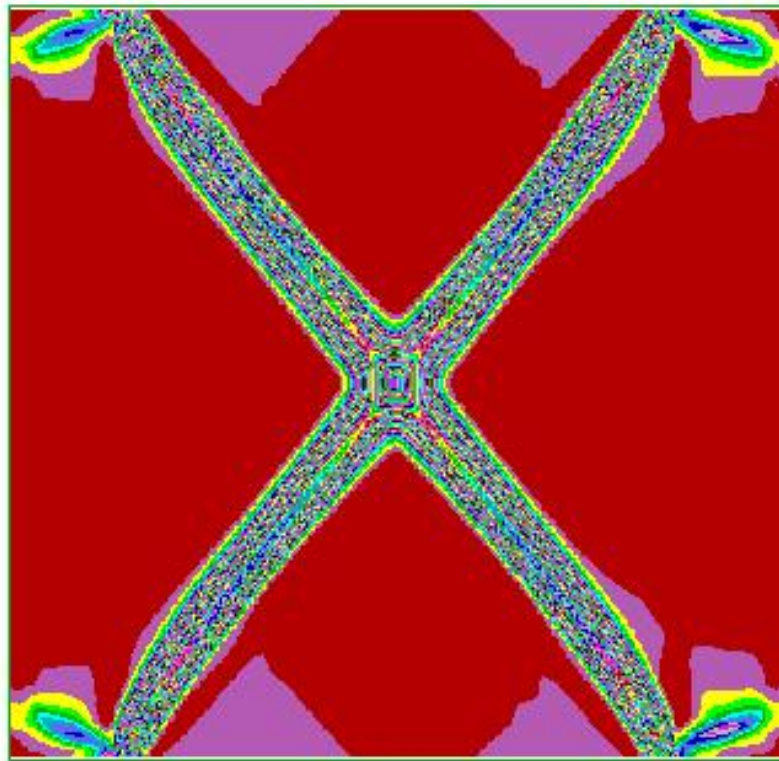


Fig. 3.19. Shear strain increment plot showing the well-developed 'conjugate' geometries. Here 'Riedel' shears are not visible due to their millimeter scale size.

3.13. Experiment 10:

In this experiment, data file was modified five times by varying the applied load or its boundary conditions to bring more deformation in the mesh.

3.13.1. Mesh size and boundary conditions

Mesh size was selected similar to the previous models 7, 8 and 9; however, variable load 200×10^2 Pa to 200×10^{10} Pa was applied to shorten the mesh. Lateral shear was also tested using the constant velocity of 3.3×10^{-5} m/steps to deform the mesh instead of vertical load, however, the required geometries were not achieved. Further variation of boundary conditions caused the complete distortion of the mesh.

3.13.2. Model run and results

Due to the similar geometries produced in every attempt, results were not saved separately. In each model, the visible 'Riedel' geometries, particularly R' shears, were not attained. The continuous development of 'conjugate' pattern in consecutive tests revealed that, it may overprint the earlier formed deformation structures i.e. 'Riedel' shears, making them obliterated in successive deformation (Fig. 3.20). The plot shown in figure 3.20 was taken by stopping the calculations at 45000 steps. This plot describes the shearing effect at a high angle of the applied load (Fig. 3.20). It is then interpreted that the formation of R' shears start first and subsequently deformed as the deformation progress. This interpretation is based on the model run and consistent with those of field examples carried out by Davies et al. 1999 and Alghran 2000.

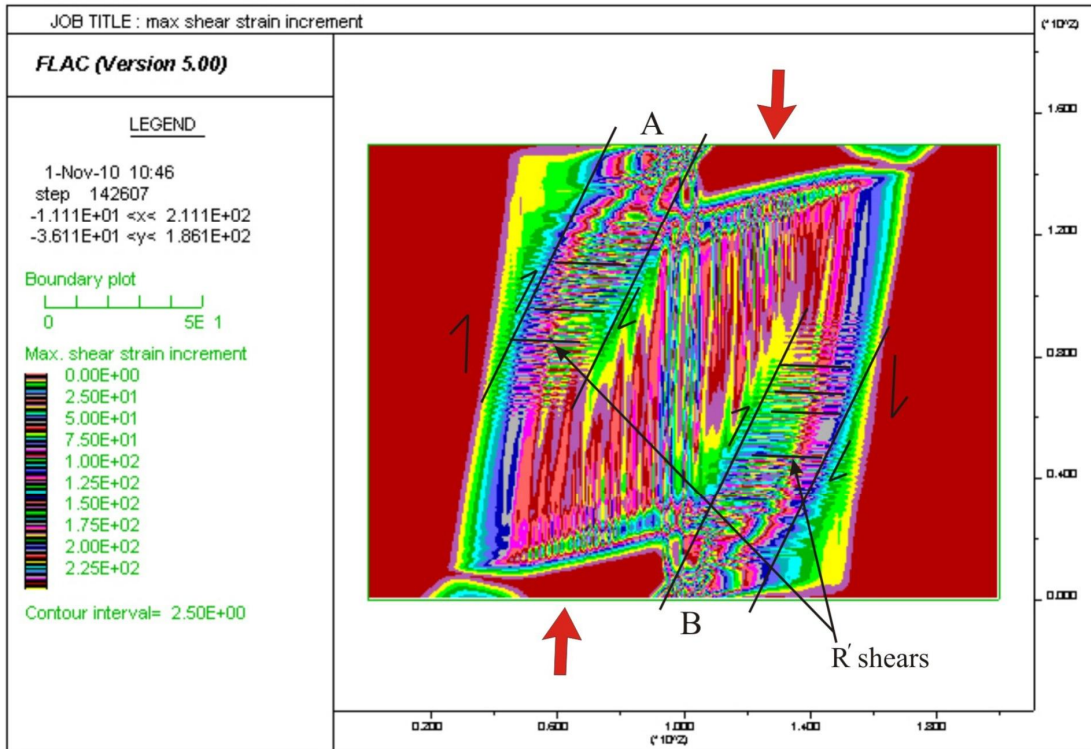


Fig. 3.20. Maximum shear strain increment plot showing the strain distribution in mesh. Note that zones 'A' and 'B' produced shear zones with $\sim 75^\circ$ shear bands, in response to differential shortening.

The results of all experiments are not shown here because there were some experiments that did not produce any sort of geometry except the distortion of entire mesh or at places mesh became invisible due to heavy stresses or boundary conditions. Applied boundary conditions matched only to the conceptual model of the problem only in experiments 6, 7, 8, 9 and 10, hence producing the required geometries.

3.14. Tabular comparison of experiments

Tabular comparisons of all the above described experiments are shown in Tables 3.4 and 3.5. These tables show the complete variation of material properties, boundary conditions, mesh size(s) and all other parameters that were used in generating the numerical model of deformation bands. Tables also differentiate between the ingredients of successful, partially successful and those experiments that did not produce any sort of geometry.

S.No	Material properties	Expr. 1	Expr. 2	Expr. 3	Expr. 4	Expr. 5	Expr. 6	Expr. 7	Expr. 8	Expr. 9	Expr. 10
1	Density (ρ) (kg/m ³)	2x10 ³	2x10 ³	2x10 ³	2.65x10 ³	2.65x10 ³	2.65x10 ³	2.65x10 ³	2.65x10 ³	2.65x10 ³	2.65x10 ³
2	Bulk modulus (K) (Pa)	26x10 ⁸	26x10 ⁸	26x10 ⁸	3.87x10 ¹⁰	2.68x10 ¹⁰	2.68x10 ¹⁰	2.68x10 ¹⁰	2.68x10 ¹⁰	2.68x10 ¹⁰	2.68x10 ¹⁰
3	Shear modulus (G) (Pa)	7x10 ⁸	7x10 ⁸	7x10 ⁸	3.96x10 ¹⁰	7x10 ⁹	7x10 ⁹	7x10 ⁹	7x10 ⁹	7x10 ⁹	7x10 ⁹
4	Friction angle (θ)	35°	35°	35°	50.6°	35°	35°	35°	35°	35°	35°
5	Tensile strength(TS) (N's/m ²)	1x10 ¹⁰	1x10 ¹⁰	1x10 ¹⁰	4.74x10 ⁶	1x10 ⁵	1x10 ⁵	1x10 ⁵	1x10 ⁵	1x10 ⁵	1x10 ⁵
6	Dilation angle (ψ)	5°	5°	5°	5°	5°	5°	5°	10°	10°	10°
7	Cohesion (C) (Pa)	1x10 ¹⁰	1x10 ¹⁰	1x10 ¹⁰	9.79x10 ⁶	1x10 ⁶	1x10 ⁶	1x10 ⁶	1x10 ⁶	1x10 ¹⁰	1x10 ¹⁰
Boundary conditions											
1	Confining Pressure (Pa)	200x10 ³	200x10 ³	200x10 ³	200x10 ³	200x10 ⁶	200x10 ³	200x10 ² -200x10 ³	200x10 ²	200x10 ²	200x10 ²
2	Applied load (Pa)	-	-	-	-	-	200x10 ² to 200x10 ⁶	200x10 ² -200x10 ⁹	200x10 ² -200x10 ⁹	200x10 ² -200x10 ⁹	200x10 ² -200x10 ¹⁰
3	Stresses (S) (Pa)	200x10 ³	200x10 ³	200x10 ³	200x10 ³	200x10 ⁶	200x10 ⁶	200x10 ⁶	200x10 ⁶	200x10 ⁶	200x10 ⁶
4	Velocity (V) (m/steps)	5x10 ⁻⁸	2.5x10 ⁻⁷	2x10 ⁻⁸	1.8x10 ⁻⁸	5.3x10 ⁻⁷	0	0	0	0	3.3x10 ⁻⁵

Table. 3.4. Table showing the variation in mechanical properties.

S.No	Experiments	Material model	Mesh size	Strain mode	Steps	Results
1	Experiment 1	Mohr-Coulomb	250x100 (2x1 m)	Large	20000	Not successful
2	Experiment 2	Mohr-Coulomb	200x100 (2x0.3 m)	Large	20000	Not successful
3	Experiment 3	Mohr-Coulomb	300x100 (2x0.6 m)	Large	50,000	Not successful
4	Experiment 4	Mohr-Coulomb	200x150 (2x1.5 m)	Large	55,000	Not successful
5	Experiment 5	Mohr-Coulomb	250x50 (0.15x0.025 m)	Large	1,00,000	Not successful
6	Experiment 6	Mohr-Coulomb	100x100 (100x100 m)	Large	102920	Partially successful
7	Experiment 7	Mohr-Coulomb	100x100 (100x100 m)	Large	101339-100040	Successful
8	Experiment 8	Mohr-Coulomb	100x100 (100x100 m)	Large	100010	Successful
9	Experiment 9	Mohr-Coulomb	100x100 (100x100 m)	Small	100010	Successful
10	Experiment 10	Mohr-Coulomb	100x100 (100x100 m)	Small	142607	Partially successful

Table. 3.5. Table showing the comparison between the mesh size, material model, strain mode and the number of steps for which solution was attained.

CHAPTER - 3

NUMERICAL SIMULATION OF DEFORMATION BANDS

CHAPTER 4

RESULTS AND COMPARISONS

In this study, numerical experiments were performed to simulate the nucleation, growth and structural evolution of ‘conjugate’ and ‘Riedel’ deformation bands in sandstone. Different experiments were carried out to examine deformation band development in a class of frictional-dilatant material (e.g. sandstone), and the results are compared with the existing analytical and numerical models. Mohr-Coulomb material model in which the material is isotropic and elasto-plastic with no hardening was adopted to model the deformation bands in FLAC-2D.

In order to calculate the formation of deformation bands in ‘conjugate’ and ‘Riedel’ pattern in FLAC, initially lateral shear was applied using velocity parameters to the mesh of 200×150 (2x1.5 m) size, the development of ‘Riedel’ pattern in sandstone is thought to be formed by lateral shearing as assumed in the theoretical and analogue models. However, surprisingly no ‘Riedel’ or ‘conjugate’ geometries were formed at any stage during lateral shearing in a given number of steps (Fig. 4.1 and 4.2).

Same experiment was repeated five times (experiment no.1, 2, 3, 4 and 5) by changing the boundary conditions i.e., constant velocity conditions and confining pressure, mesh size(s), initial mesh configuration, material properties and parameters, but the anticipated results were not achieved. Model was allowed to run in a small strain mode instead of large strain, but again failed to produce the said geometry. Model was also allowed for 100% calculations instead of specified number of steps but deformation in the mesh was not noticed.

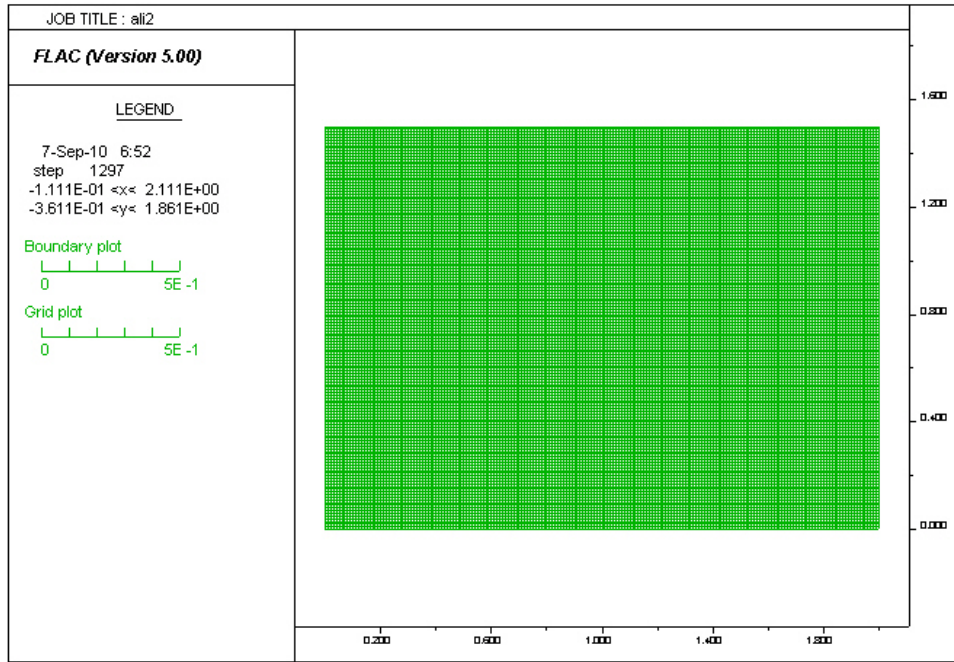


Fig. 4.1. Graph showing the geometry of the mesh before applying the boundary conditions and execution.

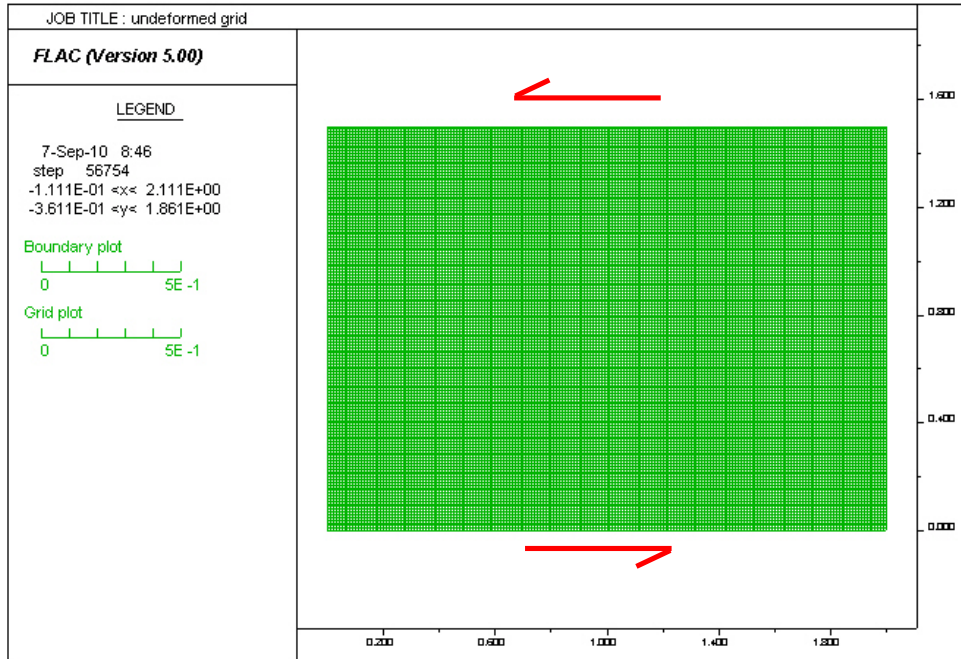


Fig. 4.2. Geometry of mesh after applying the boundary conditions and execution. Internal geometry of the mesh remains undisturbed.

Then the experimental tests carried out on cylindrical cores of rock samples, where vertical load produced ‘conjugate’ geometries (Fig. 4.3) were closely studied.

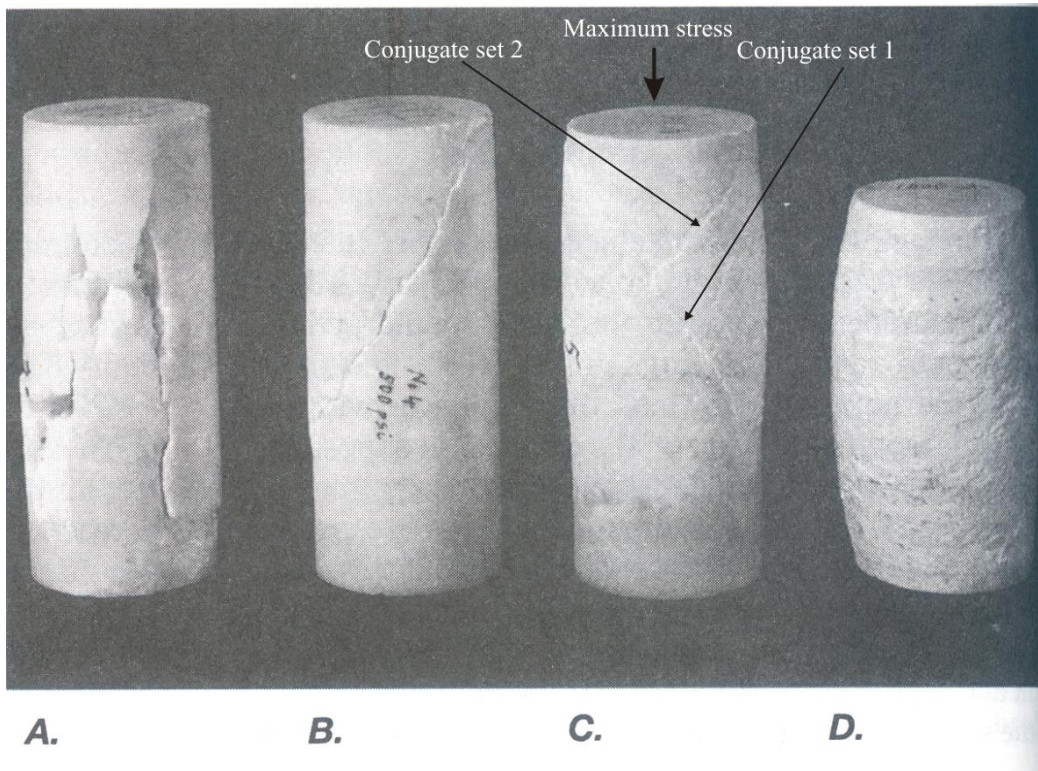


Fig. 4.3. Experimental results on cylindrical marble at room temperature.

A. longitudinal fracturing at confining pressure $P = 0.1$ MPa, B. single shear fracture at $P = 3.5$ MPa, C. conjugate sets at $P = 35$ MPa, D. ductile flow at $P = 100$ MPa (from Patterson 1978).

In subsequent runs, the experimental studies were kept in mind and applied force (σ_1) on top of the mesh (100x100 m) and observed the nucleation of ‘conjugate’ pattern (Fig. 4.4 and 4.5). Except the mesh size and boundary conditions i.e., pressure was applied in vertical direction at the top and bottom surfaces instead of lateral shear, all other properties and parameters assigned to the mesh were same to those of previous experiments (experiment no. 4 and 5). The developed pattern consists of two

cross-cutting sets oriented at an acute angle i.e. $\sim 70^\circ$ to σ_1 , and each individual set have considerable thickness i.e. 12 m (Fig. 4.5). This is consistent with the field, theoretical and experimental studies.

'Riedel' geometries may be developed within the thick deformed portions of 'conjugate' sets as discussed by Davis et al. (1999) (Fig. 2.1a). Similarly, on the basis of field studies, Sayab et al. (1999) also documented 'Riedel' sets in map-scale 'conjugate' faults in the Mochi Mar area, close to the Dara Tang fault. Shear sense of each 'conjugate' set was interpreted from the 'Riedel' fractures developed within each shear zones (Fig. 4.6). At this stage, guidelines were obtained from the clay-cake deformation experiments (Fig. 2.1b) in which horizontal load was applied to two adjoining boards overlain by a moist clay cake analogous to sedimentary cover over a basement fault. A quasi-tabular, vertical 'Riedel' shear zone was formed directly above the master fault in the overlying clay cake cover, into which the strike-slip shear strain was imposed. It was in this zone that the 'Riedel' shearing was firstly noted and described by Cools (1928) and Riedel (1929) (Fig. 2.1b). For this reason experiment 10 was executed in small strain mode. The proposed geometries formed distinct 'A' and 'B' zones with R' shears (Fig. 3.20).

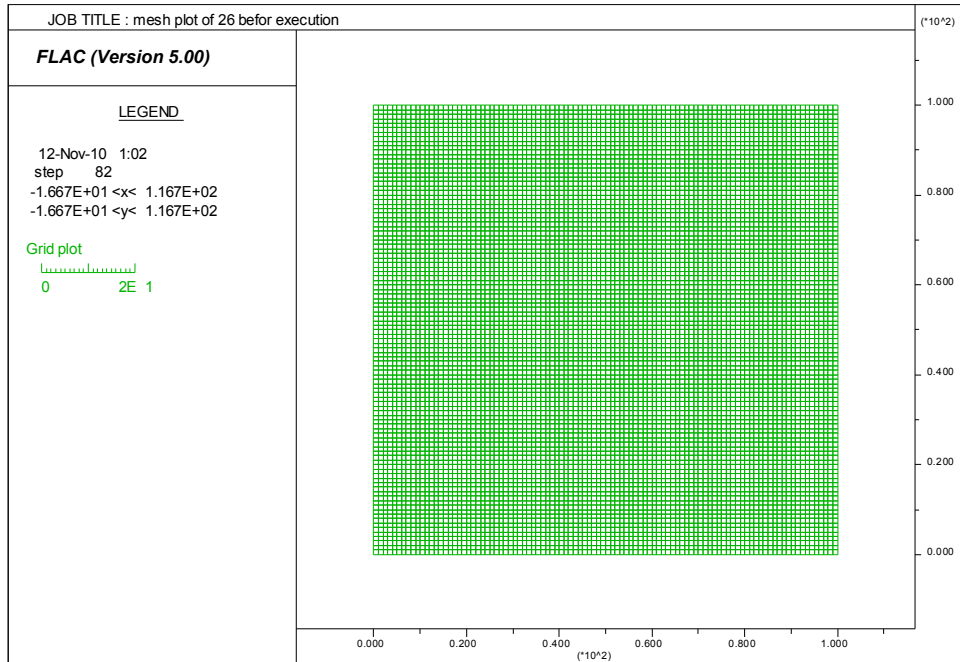


Fig. 4.4. Graph showing the geometry of 100x100 m mesh before applying the boundary conditions and execution.

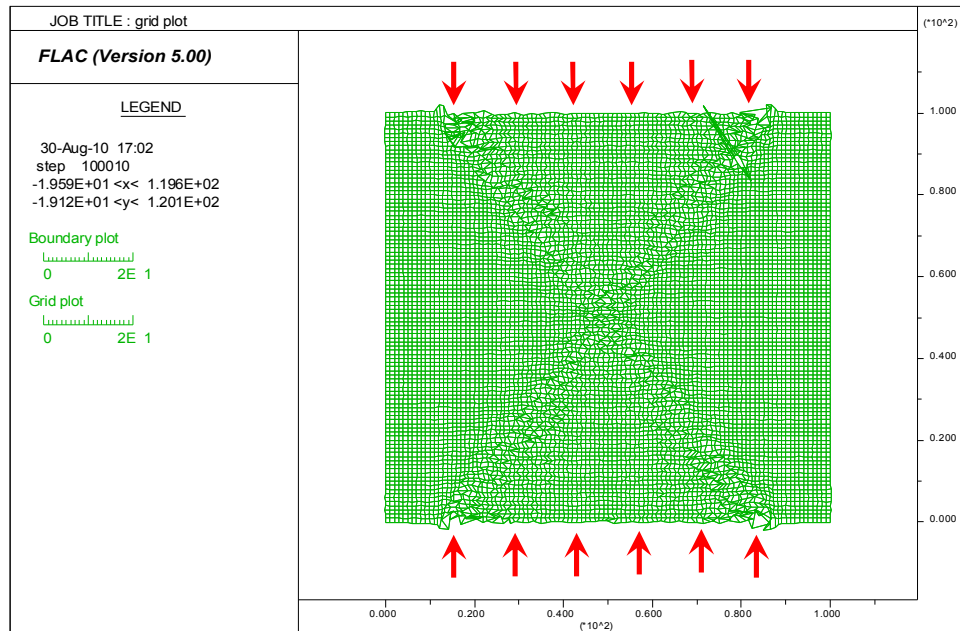


Fig. 4.5. Deformed grid after applying the load and execution. Applied load varies from 200×10^2 Pa to 200×10^9 Pa at the top and bottom surfaces. ‘Conjugate’ pattern developed at $\sim 70^\circ$. Thickness of the individual deformation band set is almost 12 m.

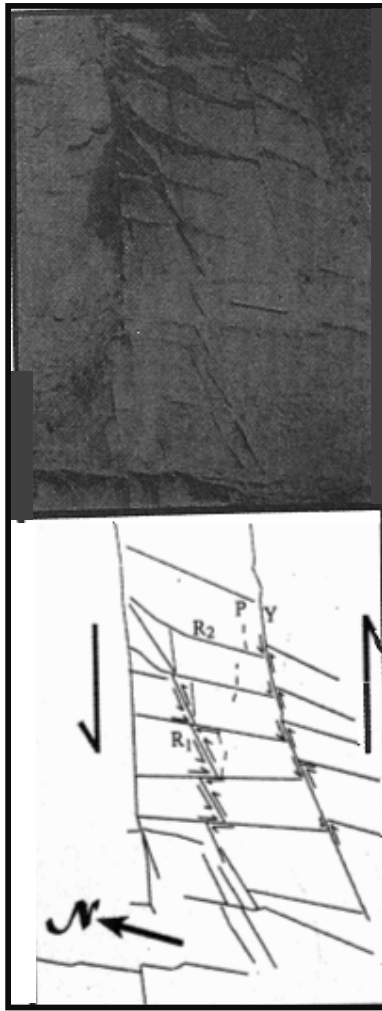


Fig. 4.6. 'Riedel' fracture pattern in deformation band shear zones in Qabul khel area (Sayab et al. 1999).

In large strain mode (experiments no. 7 and 8) 'Riedel' shears were not visible in the said model (Fig. 4.5), therefore, in order to get the clear view of these geometries, two other experiments (experiment no. 9 and 10) were carried out. In each case it was observed that deformed pattern in each 'conjugate' set was well produced but within this 12 m thick portion the millimeter scale 'Riedel' geometries were not seen though they might have developed. The continuous development of 'conjugate'

pattern in consecutive tests revealed that, it may overprint the earlier formed deformation structures i.e. ‘Riedel’ shears, making them obliterated in successive deformation (Fig. 3.20).

4.1. Comparison with other models

4.1.1. Comparison with the field models

The pattern of the numerically generated ‘conjugate’ deformation band geometry, in this study, is almost similar to the pattern proposed by Davis et al. (1999) based on field measurements (Fig. 4.7). Key similarities of both the models are listed below.

1. The numerically generated pattern consists of two cross-cutting sets oriented at an acute angle i.e. $\sim 70^\circ$ to σ_1 , which is much closed to the value proposed by Davis et al. (1999) i.e. $\sim 64^\circ$.
2. Based on field studies one cannot measure how much stress is needed to produce the ‘conjugate’ pattern in porous sandstone, however, by using numerical modeling approach, which is based on quantitative dataset, revealed 200×10^9 Pa force is needed to produce ‘conjugate’ pattern in the sample under consideration.
3. The field studies revealed that the ‘Riedel’ pattern may develop in response to ‘conjugate’ shearing. In our model, the deformed antithetic pattern in each ‘conjugate’ set may be the manifestation of R' shear. These geometries are not clearly visible due to their small-scale (mm scale), and can be visible in small strain experiments (e.g. experiment 10).

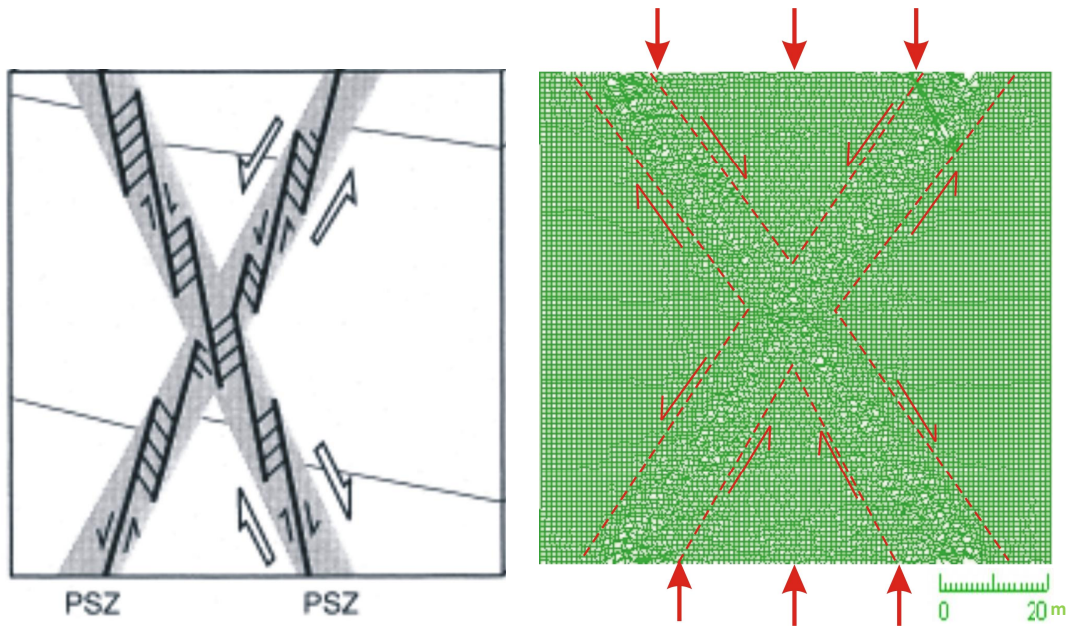


Fig. 4.7. Comparison between the model proposed by Davis et al. (1999) based on field measurements and numerically-generated ‘conjugate’ pattern.

4.1.2. Comparison with the numerical model of Hobbs and Ord (1989)

Hobbs and Ord (1989) also performed numerical modeling of shear band formation in frictional-dilatational material. Mesh size of 20x70 m was used in most of their experiments and constant velocity was used to shorten the material in plane strain between very stiff, frictionless platens for which the bulk and shear moduli were 1×10^{18} Pa. Two specimens were examined in their model. The first being homogeneous in material properties with 10 MPa cohesion, while in the second one, cohesion was given inhomogeneous distribution ranging from 0.1 MPa to 18 MPa. Elastic properties were given as shear modulus 1 GPa, bulk modulus 1 GPa and Poisson’s ratio 0.125. Only a single band (not well developed at the upper right side of the model) was generated to measure its inclination with the principal axis of compression.

However, I used a mesh of larger size (100x100 m). Finer mesh size of 250x150 (100x100 m) was also practiced for ‘Riedel’ geometries. Variable pressure (load) i.e. 200×10^2 Pa to 200×10^9 Pa was applied at the top and bottom boundaries to deform the mesh. Confining pressure of 200×10^2 Pa was also applied at the left and right side in order to confine the mesh, this resembles natural system. Homogeneous material was selected having material properties as, density 2.65×10^3 Kg/m³, bulk modulus 2.68×10^{10} Pa (26.8 GPa), shear modulus 7×10^9 Pa (7 GPa), friction angle 35°, tensile strength 1×10^5 N/m², dilation angle 10° and cohesion 1×10^6 Pa. These values are comparatively more realistic for porous sand in which deformation bands usually develop. Results close to natural and experimental studies were produced in the form of well pronounced cross-cutting bands (Fig. 4.8). I also modeled the R' shears within the ‘conjugate’ geometry in small strain mode (Fig. 3.20).

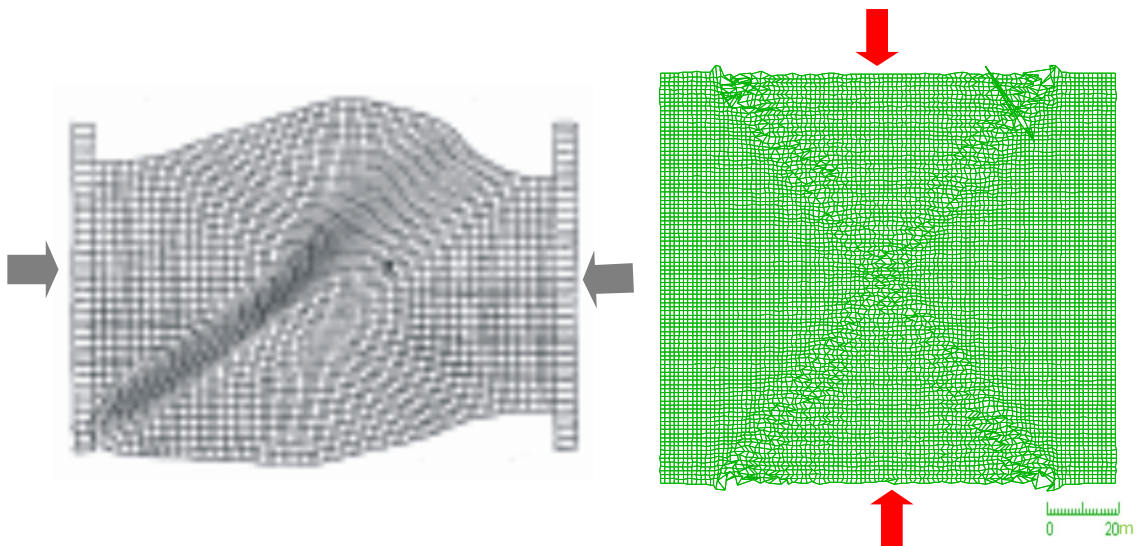


Fig. 4.8. Comparison between the numerical model generated by Hobbs and Ord., (1989) using constant velocity to shorten the mesh (left) and our model (right) of deformation bands in which variable load (200×10^2 Pa to 200×10^9 Pa) was applied to deform the mesh.

CHAPTER - 5

DISCUSSION AND CONCLUSIONS

CHAPTER 5

DISCUSSION AND CONCLUSIONS

Petroleum reservoirs are often compartmentalized by smaller scale structural elements such as deformation bands that are difficult to detect by seismic techniques, but have a profound impact on subsurface fluid movement. The geometry and spacing of the deformation band patterns ('Riedel' and 'conjugate') control shape and size of the compartments of petroleum reservoirs. So the detail knowledge of deformation band geometries i.e., 'conjugate' and 'Riedel' fault geometries, is helpful in modeling the influence of compartmentalization on fluid flow in sandstone reservoirs, especially where sandstones are highly porous and the favored mechanism of deformation is the development of deformation bands. Deformation band shear zones are marked by significant reduction in porosity of the host lithology, and thus they form impermeable barriers to fluid flow within otherwise porous, permeable reservoir rock (Antonellini et al., 1994; Antonellini and Aydin, 1994). Therefore, understanding the mechanism of deformation band formation is important in fluid flow modeling.

On the basis of present study, following points were concluded:

1. 'Conjugate' pattern developed at an acute angle $\sim 70^\circ$ to σ_1 , which is much closed to $\sim 64^\circ$, the value proposed by Davis et al. (1999).
2. Thickness of the individual deformation band set in 'conjugate' pattern is almost 12 m. This thickness depends on a number of factors including applied load, density of the rock sample, configuration of the mesh etc...
3. The 'Riedel' geometry may form along 'conjugate' bands (that are lying at an acute angle to σ_1) due to lateral shearing.

4. Deformed antithetic pattern in each 'conjugate' set may be the manifestation of R' shear. These geometries are not clearly visible due to their smaller size i.e. millimeter scale and they may be overprinted by the development of 'conjugate' pattern.
5. This modeling technique can be applied effectively to model other structural systems i.e. thrust faults, strike-slip faults of smaller- to larger- scale with far ranging applications especially in petroleum exploration and production, and in hydrogeology.
6. Assigned boundary conditions can cause numerical error if parameters value exceeds the some specific value. Hence, care should be taken.
7. At a constant value of friction angle, 'conjugate' pattern of deformation bands become more pronounced as the value of dilation increases during the simulation.
8. Development of deformation bands in the mesh is strongly dependent upon the size of mesh, more finer the mesh more pronounced will be the geometries.
9. Based on field investigations one cannot deduce how much stress is needed to produce 'conjugate' pattern in porous sandstone, however, by using numerical modeling approach, which is based on quantitative dataset, revealed $200 \times 10^9 \text{Pa}$, a value responsible for generating deformation bands in the sample under consideration.
10. The numerical simulation is a powerful technique to monitor results in various steps.

REFERENCES

- Ahlgren, S. G., 2001. The nucleation and evolution of Riedel shear zones as deformation bands in porous sandstone. *Journal of Structural Geology*, 23, 1203–1214.
- Anderson, E. M., 1942. *The Dynamics of Faulting and Dyke Formation with application to Britain*, Oliver and Boyd, Edinburgh, London.
- Antonellini, M. A., Aydin, A., Pollard, D. D., 1994. Microstructure of deformation bands in porous sandstones at Arches National Park, Utah. *Journal of Structural Geology*, 16, 941–959.
- Antonellini, M., Aydin, A., 1994. Effect of faulting on fluid flow in porous sandstones: petrophysical properties. *AAPG, Bulletin* 78, 355–377.
- Antonellini, M., Du, Y., Aydin, A., Pollard, D. D., 1992. Evolution of faults in sandstone and their permeability. *Geological Society of America Abstracts with Programs* 24, 157.
- Aydin, A., 1978. Small faults formed as deformation bands in sandstone. *Pure and Applied Geophysics*, 116, 913–930.
- Aydin, A., Borja, R. I. and Eichhubl, P., 2006. Geological and mathematical framework for failure modes in granular rock. *Journal of Structural Geology*, 28, 83–98.
- Aydin, A., Johnson, A. M., 1978. Development of faults as zones of deformation bands and as slip surfaces in sandstone. *Pure and Applied Geophysics*, 116, 931-942.

- Aydin, A., Johnson, A. M., 1983. Analysis of faulting in porous sandstones. *Journal of Structural Geology*, 5, 19-31.
- Azizullah., 1995. Petrotectonic, petrology and genesis of uranium mineralization of the Siwalik Group of Thatti-Nasratti and Shava-Shanawah area. Unpublished Ph. D. thesis, Punjab University.
- Baker, D. M., Lillie, R. J., Yeats, R. S., Johnson, G. D., Yousuf, M., Zaman, A. S. H., 1988. Development of the Himalayan thrust zone: Salt Range, Pakistan. *Geology*, 16, 3-7.
- Bartlett, W. L., Friedman, M., Logan, J. M., 1981. Experimental folding and faulting of rocks under confining pressure, Part IX: Wrench faults in limestone layers. *Tectonics*, 79, 255-277.
- Bergbauer, S., Pollard, D. D., 2004. A new conceptual fold fracture model including pre folding joints, based on the Emigrant Gap anticline, Wyoming. *Geological Society of America*, 119, 294-307.
- Billi, A., 2005. Attributes and influence on fluid flow of fractures in foreland carbonates of southern Italy. *Journal of Structural Geology*, 27, 1630-1643.
- Billi, A., Salvini, F., Storti, F., 2003. The damage zone-fault core transition in carbonate rocks: implications for fault growth, structure and permeability. *Journal of Structural Geology*, 25, 1779–1794.
- Braun, J., 1994. Three-dimensional numerical simulations of crustal-scale wrenching using a non-linear failure criterion. *Journal of Structural Geology*, 16, 1173-1186.
- Buck, W. R., Lavier, L., Poliakov, A., 2005. Modes of faulting at mid-ocean ridges. *Nature*, 434, 719–723.

- Byerlee, J. D., Brace, W. F., 1968. Stick slip, stable sliding, and earthquakes- effect of rock type, pressure, strain rate, and stiffness. *Journal of Geophysical Research*, 73, 6031-6037.
- Cloos, E., 1955. Experimental analysis of the fracture pattern. *Geological Society of America Bulletin*, 66, 241-256.
- Cotter, G. P., 1933. The geology of the part of the Attock District, West of Longitude 72° 45'E. *Geol. Surv. India, Mem.* 55: 63-161.
- Danilchik, W., Shah, S. M. I., 1987. Stratigraphy and coal resources of the Makarwal area, Trans-Indus mountains, Mianwali District, Pakistan. *U.S. Geological Survey Professional Paper*, 1341, 1-139.
- Davis, G. H., 1996. 'Riedel relays' in deformation band shear zones, Colorado Plateau, Utah. *Geological Society of America Abstracts with Programs*, 28, A-188.
- Davis, G. H., Bump, A. P., García, P. E., Ahlgren, S. G., 1999. Conjugate Riedel deformation band shear zones. *Journal of Structural Geology*, 22, 169–190.
- Fay, C., Bell, T. H., Hobbs, B. H., 2008. Porphyroblast rotation versus non-rotation: Conflict resolution! *Geology*, 36, 307-310.
- Fossen, H., 2010. Deformation bands formed during soft-sediment deformation: Observations from SE Utah. *Marine and Petroleum Geology*, 27, 215–222.
- Fossen, H., Hesthammer, J., 1997. Geometric analysis and scaling relations of deformation bands in porous sandstone. *Journal of Structural Geology*, 19, 1479–1493.
- Fossen, H., Schulz, R. A., Shipton, Z. K., Mair, K., 2007. Deformation bands in sandstone: a review. *Journal of the Geological Society London*, 164, 755–769.

- Friedman, M., Logan, J. M., 1973. Lu "ders' bands in experimentally deformed sandstone and limestone. *Geological Society of America Bulletin*, 84, 1465–1476.
- Fullsack, P., 1995. An arbitrary Lagrangian–Eulerian formulation for creeping flows and its application in tectonic models. *Geophysical Journal International*, 120 (1), 1-23.
- Garcia, P., Davis, G. H., 1997. Detailed internal structure of a conjugate normal deformation band shear zone system in the Navajo sandstone at the northern end of the east Kaibab monocline, southern Utah. *EOS, Transactions of the American Geophysical Union*, 78, F702.
- Gee, E. R., 1989. Overview of the geology and structure of the Salt Range, with observation on related areas of northern Pakistan. *Geological Society of America Special Paper*, 232, 95-112.
- Gerbault, M., Burov, E. B., Poliakov, A. N. B., Daignieres, M., 1999. Do faults trigger folding in the lithosphere? *Geophysical Research Letters*, 26 (2), 271–274.
- Hobbs, B. E., Ord, A., 1989. Numerical simulation of shear band formation in a frictional dilational material. *Ingegneria e l'architetto*, 59, 209–220.
- Itasca Consulting Group. Minneapolis, Minnesota, Itasca Consulting Group, Inc 2006, FLAC3D Version 3.10.
- Johnson, S. E., 2009. Porphyroblast rotation and strain localization: Debate settled. *Geology*, 37, 663 - 666.
- Khan, M. J., Opdyke, N. D., 1987. Magnetic-polarity Stratigraphy of the Siwalik Group of the Shinghar and Surghar Range, Pakistan. *Geological Bulletin University of Peshawar*, 20, 111-127.

- Kamran, M. A., Ahmad, N., Islam, W., 2006. Sequential development of syn-folding joint patterns and post-folding fault related Deformation Band Shear Zones: implications for determining regional kinematics history of the southern Surghar-Shinghar Range, Pakistan. Unpublished M.Sc thesis, university of Peshawar.
- Lucas, S. E., Moore, J. C., 1986. Cataclastic deformation in accretionary wedges: Deep Sea Drilling Project Leg 66, southern Mexico, and on-land examples from Barbados and Kodiak Islands. In: Editor, A. (ed.) Book title. Geological Society of America, Memoirs, 166, 89–103.
- Mair, K., Main, I., 2000. Sequential growth of deformation bands in the laboratory. *Journal of Structural Geology*, 22, 25–42.
- Marti, J., Cundall, P., 1982. Mixed Discretization Procedure for Accurate Modeling of Plastic Collapse. *Int. J. Num. & Analy. Methods in Geomechanics*, 6, 129-139.
- McLellan, J. G., Oliver, N. H. S., Schaub, P. M., 2004. Fluid flow in extensional environments; numerical modelling with an application to Hamersley iron ores. *Journal of Structural Geology*, 26, 1157–1171.
- Mollema, P. N., Antonellini, M., 1996. Compaction bands; a structural analog for anti-mode I cracks in aeolian sandstone. *Tectonophysics*, 267, 209-228.
- Okubo, C. H., Schultz, R. A., 2005. Evolution of damage zone geometry and intensity in porous sandstone: insight gained from strain energy density. *Journal of the Geological Society of London*, 162, 939-949.
- Olsson, W. A., 2000. Origin of Lu "ders' bands in deformed rock. *Journal of Geophysical Research*, 105, 5931–5938.

- Olsson, W. A., Lorenz, J. C., Cooper, S. P., 2004. A mechanical model for multiply-oriented conjugate deformation bands. *Journal of Structural Geology*, 26, 325–338.
- Paterson, M. S., 1978. *Experimental rock deformation- The Brittle Field*. New York, Springer Verlag.
- Pilgrim, G. E., 1913. The correlation of the Siwaliks with mammal horizons of Europe. *Ind. Geol. Surv. Res.*, 43(2): 264-326.
- Poliakov, A., Podladchikov, Y., Dawson, J. B., Talbot, C., 1996. Salt diapirism with simultaneous brittle faulting and viscous flow. *Geological Society Special Publication*, 100, 291–302.
- Riedel, W., 1929. Zur mechanik geologischer brucherscheinungen, *Centralblatt für Mineralogie, Geologie, und Paleontologie*, 354-369.
- Rotevatn, A., Buckley, S. J., Howell, J. A., Fossen, H., 2009. Overlapping faults and their effect on fluid flow in different reservoir types: A LIDAR-based outcrop modeling and flow simulation study. *AAPG*, 93, 407- 427.
- Sayab, M., But, K. A., Khan, M. A., Rafiq, M., 2001a. Parallel, sub-parallel drainage pattern in the Surghar-Shinghar Range controlled by neo-tectonic extension fractures associated with Main Frontal Thrust. 4th Pakistan Geological Congress. Abstracts, 73-74.
- Sayab, M., Khan, M. A., But, K. A., Pervaiz, K., 1999. Analysis of the joint and associated Neo-tectonic deformation band shear zones in the Siwalik group of southern Surghar-Shinghar range, Trans-Indus range, Pakistan. *Geological Bulletin University of Peshawar*, 32, 25-39.
- Sayab, M., Mazhar, F., But, K. A., Khan, M. A., 2001b. Structure of the Surghar Range at its south eastern flank with emphasis on Surghar Thrust. 4th Pakistan Geological Congress. Abstracts, 38-39.

Schultz, R. A., Balasko, C. M., 2003. Growth of deformation bands into echelon and ladder geometries. *Geophysical Research Letters*, 30, 20, 2033, doi:10.1029/2003GL018449.

Schultz, R. A., Siddharthan, R., 2005. A general framework for the occurrence and faulting of deformation bands in porous granular rocks. *Tectonophysics*, 411, 1-4, 1-18.

Shimizu, Y., Hart, R., Cundall, P., 2004. *Numerical Modeling in Micromechanics via Particle Methods*, Taylor & Francis group plc, London, UK, 435p.

Shipton, Z., Cowie, P. A., 2001. Damage Zone and Slip-Surface Evolution over Micro- to Kilometre Scales in High-Porosity Navajo Sandstone, Utah. *Journal of Structural Geology*, 23, 1825-1844.

Torabi, A., 2007. Deformation bands in porous sandstones, their microstructure and petrophysical properties. Ph.D. thesis, Department of Earth Science university of Bergen, Bergen, Norway, 149p.

Uzkeda, H., Poblet, J., Bulnes, M., 2010. A geometric and kinematic model for double-edge propagating thrusts involving hangingwall and footwall folding. An example from the Jaca–Pamplona Basin (Southern Pyrenees). *Geological Journal*, 45, 5-6, 506–520.

Web link: <http://www.ig.tuwien.ac.at/forschung/schwerpunkte/deformation-mechanism-in-porous-sediments.html>

Woodcock, N., Schubert, C., 1994. Continental strike-slip tectonics. In: Hancock, P. (Ed.), *Continental deformation*. Pergamon Press, New York, pp. 251-263.

Yeats, R. S., Khan, E. H., Akhtar, M., 1984. Late Quaternary deformation of the Salt Range, Pakistan. *Geological Society of America, Bull.* 95, 958-966.